Food product quality measurement and visualization using fluorescence fingerprint

(蛍光指紋による食品品質の計測と可視化)

January, 2021

Doctor of Philosophy (Engineering)

Bui Minh Vu

ブイミンブー

Toyohashi University of Technology

Abstract

Public interest in food quality and production has increased in recent decades. This increase is probably related to the changes in eating habits, consumer behavior, and the development and increased industrialization of the food supply chains. The demand for high quality and safety in food production calls for high standards for quality and process control, which requires sensitive and rapid analytical tools to investigate the food. An excitation-emission matrix (EEM), also known as fluorescence fingerprint, has been widely applied for the nondestructive measurement of the physical and chemical properties of objects. Determination of the food quality using fluorescence measurements have been achieved with high accuracy in many previous studies. However, adopting fluorescence as a technique for determining the quality and authenticating food products is still limited due to the high cost involved. This thesis presents the novel imaging method using fluorescence and presents universal band-pass filters made suitable for their introduction in the food industry.

First, a novel fluorescence imaging method was developed by combining the excitation-emission matrix (EEM) and imaging techniques to visualize the spatial-temporal changes of K-value and IMP. The result showed that the distribution of K-value-value and IMP content could be visualized with an accuracy of $R^2 = 0.78$ and $R^2 = 0.83$, respectively. Furthermore, this innovative approach was applied to differentiate burnt meat, which is a type of abnormal meat found in many types of fish, and it was found that burnt meat could be detected even when in a frozen condition.

Next, the versatile band-pass filters for fluorescence imaging of food product for quality assessment was defined by simulation. The results showed that the proposed band-pass filters are able to reduce the number of variables in the prediction model, thereby reducing the measurement time and filter cost while having similar or practical accuracies in most of the cases such as estimating aflatoxin contamination in nutmeg, inosine 5'-monophosphate (IMP) of frozen fish and geographical origin of mangos compared to the methods reported previously.

As a conclusion, this thesis proposed a novel method to apply fluorescence as a food quality assessment. The proposed fluorescence imaging method and versatile band-pass filters offer a more practical way of adopting fluorescence as a technique for determining the quality and authenticating food products instead of using point measurements or searching the target-dependent excitation-emission wavelength combinations.

Acknowledgments

I would like to express my deep and sincere gratitude to my supervisor, Prof. Shigeki Nakauchi, for the continuous support of my Ph.D study and research, for his patience, motivation, enthusiasm and immense knowledge.

I am extremely grateful to my external supervisor, Dr. Mizuki Tsuta, Food Research Institute, Food Research Institute, National Agriculture and Food Research Organization, for his dedicated consistent support and guidance. He was always willing and enthusiastic to assist in any way he could throughout the thesis.

I also would like to thank Prof. Tetsuto Minami, and Assoc. Prof. Kyoko Hine for their professional and scientific advice and administrative support. Nevertheless, I would like to thank Mrs. Yuki Kawai for her support daily through laboratory life.

Finally, I am very grateful for my family and my friends for their patience and support.

Contents

List of Figures

List of Tables

Chapter 1

Introduction

In recent decades, public interest in food quality and production has increased. This increase is probably related to the changes in eating habits, consumer behavior, and the development and increased industrialization of the food supply chains. The demand for high quality and safety in food production calls for high standards for quality and process control, which requires sensitive and rapid analytical tools to investigate the food [1]. In order to solve this problem, optical methods are currently attracting attention. Optical methods utilize absorption and radiation caused by the interaction of light such as ultraviolet, visible, and infrared light with the object [2], and can be used for analysis without any pretreatment (such as using chemicals, deforming or damaging the object), thus enabling fast inspection.

An excitation-emission matrix (EEM), also known as fluorescence fingerprint [3], is a set of fluorescence spectra acquired at consecutive excitation wavelengths to create a three-dimensional diagram. The EEM has been widely applied for nondestructive measurement of physical and chemical properties of objects [4–7]. In food products quality assessment, EEM is able to determine several properties (functional, composition, nutritional, and origin) of animal (for example dairy, meat, fish, and egg) and vegetable (oils, cereal, sugar, fruit, and vegetable) products as well as the identification of bacteria of agro-alimentary interest without the use of chemical reagents [8]. The determination of a chemical property or the classification of the geographical origin of food can be carried out with high accuracy using EEM. In recent years, numerous EEM related methods and applications have been published. However, the corresponding actual innovations are still not significant in the food industry. This is because adopting fluorescence as a technique for determining the quality and authenticating food products in the industry is still limited.

This thesis presents the novel imaging method using fluorescence and presents universal band-pass filters made suitable for their introduction in the food industry. Chapter 3 presents a novel fluorescence imaging

method was developed by combining the excitation-emission matrix (EEM) and imaging techniques. This approach based on expanding the point estimation of EEM to the image, where each point in EEM corresponds to one image measured under a specific excitation-emission wavelength. An optimization method also proposed to reduce the dimensions of the EEM by selecting the most efficient excitation wavelength, which allows visualizing the target using only one excitation light. The proposed fluorescence imaging method was applied to visualize the spatial-temporal changes of the freshness indices (K-value) and taste component (IMP) content in frozen fish. Furthermore, this innovative approach was applied to differentiate burnt meat, which is a type of abnormal meat found in many types of fish. Chapter 4 presents the versatile band-pass filters for fluorescence imaging of food product for quality assessment was defined by simulation. In the first phase, 70 compounds related to food nutrition, freshness, and umami components were selected as samples for fluorescence spectra (EEM) measurement. From the obtained EEM, a synthetic EEM dataset was generated. Parallel factor analysis (PARAFAC) was applied to the generated synthetic EEM dataset in order to define the excitation-emission wavelength of the band-pass filters. In the second phase, the practicality of the proposed band-pass filters was verified by employing them to solve a real problem. Finally, the outcomes of this thesis were summarized in Chapter 5 as the conclution.

Chapter 2

Excitation-emission matrix and fluorescence imaging

2.1 Light and spectrum

Light is a collection of electromagnetic waves of various wavelengths. Light of different wavelengths appears as different colors to the human eye. Humans can only perceive light of visible wavelengths (380 to 780 nm) as colors, which is a very narrow range of electromagnetic waves. Electromagnetic waves are classified into radio waves, infrared, light (visible light), ultraviolet, X-rays, gamma rays, and cosmic rays according to their wavelengths, and each has its own characteristics (Fig. 2.2.1). The order of those wavelengths is called the spectrum.

2.2 Spectroscopy

Spectroscopy is the study of identifying and quantifying the components of the substance by examining the spectrum of light emitted, absorbed, or reflected from substance. When a substance is illuminated by light, the energy state of the atoms that make up the substance shifts from a low energy state (ground state) to a high energy state (excited state), where absorption occurs. The electrons in atoms are excited in different orbitals in high energy light such as UV and visible light, while they are excited in the same orbitals in low energy light such as infrared light.

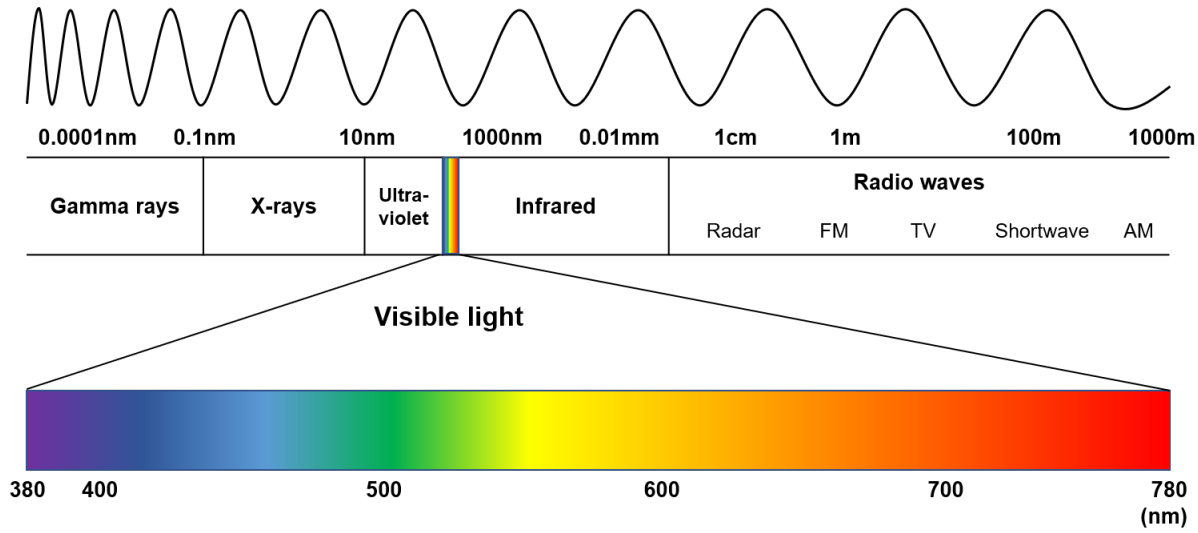

Fig. 2.2.1: Wavelengths of electromagnetic waves and light.

In both cases, when the energy input is cut off, a reverse transition from the excited state to the ground state occurs, and light is emitted according to the energy absorbed in this process. The frequencies of the absorbed and emitted light are very selective with respect to the type and structure of atoms and molecules, and thus the absorption and emission spectra can be used for the identification and quantification of materials. The advantages of spectroscopy are as follows [2].

- Since no chemicals are used, the analysis costs are low and there is no risk of environmental contamination by chemicals
- No preprocessing is required, allows rapid analysis
- The same sample can be measured repeatedly
- No special skill is required for analysis
- Short analysis time and suitable for quality monitoring
- Allows multiple items of information to be obtained simultaneously, making it possible to measure overall quality characteristics

2.3 Fluorescence spectroscopy

Fluorescence is a phenomenon in which a substance, when irradiated (excited) by light of a certain wavelength, absorbs this light and emits light of a longer wavelength [9]. Fluorescence spectroscopy is a method of taking out only the fluorescence from a sample excited by illumination and observing it [9]. There are two type of fluorescence spectrocopy: autofluorescence method, which uses the inherent fluorescence of the specimen; and secondary fluorescence method, which stains the specimen with a fluorescent dye. Since the fluorescence intensity is very weak compared to the excitation light, the excitation light must be completely cut off during observation. For this reason, an excitation filter that selects the excitation wavelength is placed in the illumination side and an absorption filter that transmits only the fluorescence is placed in the observation side. Fluorescence spectroscopy is characterized by its high sensitivity in principle compared to other absorption-based spectroscopy.

2.3.1 Excitation-emission matrix (EEM)

An excitation-emission matrix (EEM), also known as fluorescence fingerprint, is a set of fluorescence spectra acquired at consecutive excitation wavelengths to create a three-dimensional diagram [3]. EEM is widely used in biological sciences due to its high sensitivity and specificity.

Food contains a wide range of fluorescent compounds which are important for nutritive, compositional, and technological quality. Therefore, food usually has complex chemical properties which in most cases include several intrinsic fluorophores and other phenomena that influence the targeted fluorescence signal. EEM has been widely applied to handle the complex fluorescence properties of food, due to the features described abrove. For example in meat [10–12], fish [13–16], egg [17, 18], fruit and vegetable [19–23], edible oils [24–27], beer [28–32]. Even though many methods have been proposed in previous studies and have achieved high accuracy, challenges still exist regarding the implementation of this technology at the food industry level. Firstly, most of the previous studies are point measurements, which can not measure the whole and multiple samples at the same time. This means that it is not suitable for food product measurement, which has a large distribution volume. Secondly, different wavelengths are chosen for different estimation targets in the calibration stage. Therefore, different band-pass filters are needed for different estimation targets, making it a costly technique and not practical use.

Chapter 3

Visualize the quality of frozen fish

3.1 Introduction

Freshness is regarded as one of the vital parameters for the quality assessment of fish and fish products. With the increasing globalization of the sale of fish products, the demand for frozen marine products, such as tuna, mackerel, cod, salmon etc., is increasing day by day. Therefore, the quality monitoring of frozen marine products has become essential in the fishery industry, and efficient and effective quality assurance is becoming increasingly important. Improved methods for determining freshness and quality are sought by processors, consumers, and regulatory officials [33]. Nowadays, attention is focused on developing rapid, reliable and non-destructive techniques at moderate costs for monitoring seafood quality and freshness to verify that it is safe for human consumption. A number of sensory and instrument methods have been proposed to evaluate the state of fish freshness [34, 35]. Sensory methods require trained personnel and is somewhat time consuming, and therefore are considered costly and not always practical for large-scale commercial purposes. As chemical and biochemical methods for the evaluation of freshness eliminate personal opinions in quality scoring based on organoleptic changes occurring as fish storage time is extended, they are, accordingly, considered more reliable and accurate than sensory methods.

In the chemical methods, concentrations of adenosine 5'-triphosphate (ATP) and its breakdown products, which are adenosine 5'-diphosphate (ADP), adenosine 5'-monophosphate (AMP), inosine 5'-monophosphate (IMP), inosine (HxR), and hypoxanthine (Hx), respectively, are used as indices of freshness quality in a wide variety of fish [36–41]. The ratio among all or some of these nucleotide breakdown compounds are commonly used as indicators of freshness quality. The IMP content increases after decomposition of ATP and decreases after maintaining for a certain period of time and is well known

as a component strongly related to the "umami taste" of fish [42]. K-value, which is defined as the ratio of non-phosphorylated ATP metabolites to the total ATP breakdown products, was suggested in 1958 by a Japanese research group as an objective index of fish freshness [43].

Traditional methods using either sensory or instrumental evaluation, can provide reliable information about fish quality, however, these methods are destructive, expensive, time-consuming, and require highly skilled personnel. Note that, once fresh and un-fresh fish are frozen, they generally look the same and it would be rather difficult to differentiate them with the naked eye. Moreover, we must consider the influence of thawing when frozen fish is evaluated. The only way to discover the difference between fresh and un-fresh states either optically or destructively is by using conventional chemical analyses on frozen fish. In fish quality assessment, EEM has been applied to estimate freshness indices (such as K-value) and ATP content in frozen fish with high precision [14–16]. However, this approach is a point measurement which can only estimate quality at one point, and the freshness condition of other parts of fish body could not be tracked. Therefore, the previous methods are not practical for large-scale commercial purposes such as that of mackerel, which involves a vast number of fish and whose freshness declines quickly, or a big fish such as tuna, where the progress of freshness change varies for individual fish, lots, and parts.

In this study, we focus on a novel fluorescence imaging method, in which EEM is combined with imaging techniques, to visualize the distribution of fish quality such as K-value and IMP content. This approach based on expanding the point estimation of EEM to image, where each point in EEM corresponds to one image measured under a specific excitation-emission wavelength. We also propose an optimization method to reducing the dimensions of the EEM by selecting the most efficient excitation wavelength, which allow us to visualize both K-value and IMP content using only one excitation light. Firstly, we prepared fish samples with different freshness conditions, then measured the fluorescence spectra (EEM) and the fish quality (K-value and IMP content) of the samples. By using the measured EEM data to estimate K-value and IMP content, the most efficient excitation wavelength was selected for visualization. After that, we measured fluorescence images under the most efficient excitation wavelength and then built the visualization model from the measured fluorescence images.

In experiment 2, the obtained visualization model was applied to solve the on-site problem. In previous studies, it has been reported that the quality of fish depends on the killing procedures. In general, fishes in the market are caught with fishing nets and some of them likely die while struggling in them. The result of a violent struggle during capture makes muscle soften faster and could not be eaten raw in the struggled samples compared to instantly killed samples [44]. This problem, which known as "burnt meat" or, in

Japanese, as "yake niku", is a type of abnormal meat that occurs in many types of fish such as tuna, amberjack, mackerel etc. Instead of being translucent, firm and possessing a delicate flavor, burnt meat is pale, exudes a clear fluid, and has a soft texture and slightly sour taste [45]. However, burnt fish and instantly killed fish generally look the same when frozen and is somewhat difficult to differentiate them using the naked eye. In experiment 2, the visualization model obtained in experiment 1 was applied to identify burnt fish samples.

3.2 Material and methods

3.2.1 Experiment 1

Fish samples

The first group of alive spotted mackerel (*Scomber australasicus*) with an average weight of 341±72.3 g and length of 29.9±1.9 cm was harvested from a fish cage (Kamaishi City, Iwate Prefecture, Japan). Twenty four fresh fish were immediately killed by neck breaking, put in slurry ice for blood removal as well as to minimize the changes of the freshness condition and were then transferred to the laboratory. All fish samples were beheaded, gutted, had their tail cut and then vacuum packed. Three samples were filleted, vacuum packed and immediately frozen, while the rest were stored in iced water in a low temperature room at 1 °C for 3.5 h, 1, 2, 3, 5, 7, 9 days to simulate the different freshness conditions, then filleted, vacuum packed and frozen by air blast freezer at −60 °C. There were eight different freshness conditions and three spotted mackerel were used for each condition, yielding 24 fillets of the left-side and 24 fillets of the right-side. The left-side fillets were used to measure EEM and ATP-related compounds, and the right-side fillets were used to measure fluorescence image.

Fluorescence spectra (EEM) measurement

The fluorescence spectra of the frozen fillets were measured by using a fluorescence spectrophotometer F-7000 (Hitachi High-Tech Science Corporation). In this experiment, the left-side fillets were used and placed inside the portable freezer with dry ice to maintain the temperature of samples and environment below −30 °C. EEM data at two points (A, B) as shown in Fig. 3.2.1 were measured using an external Y-type fiber optic probe. At each point, EEM was obtained by measuring the emission intensity in 10 nm intervals between 250~800 nm while scanning the excitation wavelengths from 250~800 nm in 10 nm steps. The slit width was set at 20 nm for both excitation and emission and scan speed was set at 30 000 nm/min. The photomultiplier voltage (PMT voltage) was adjusted to 350 V throughout the entire experiment.

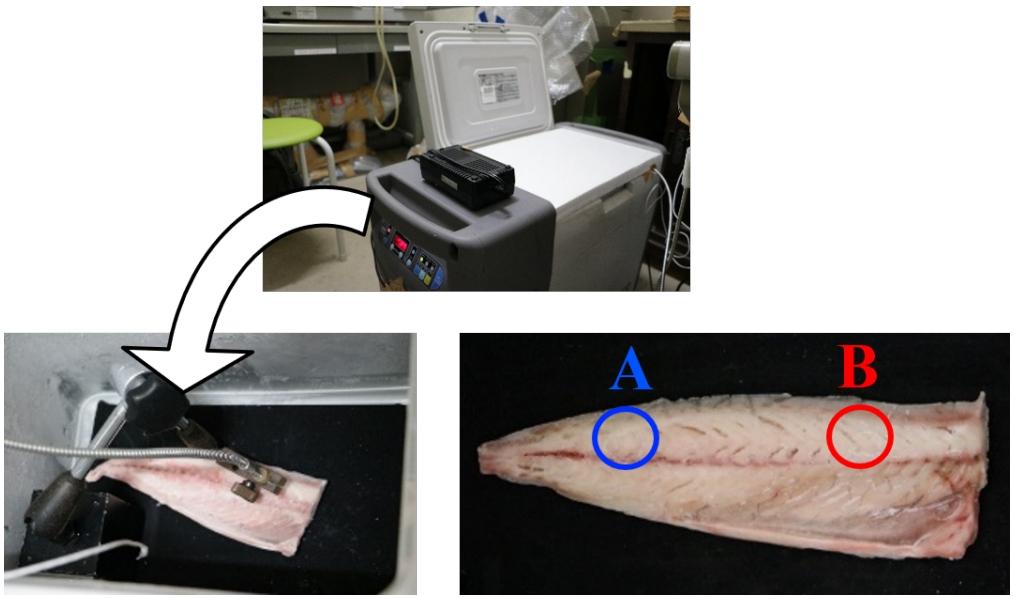

Fig. 3.2.1: EEM measurement environment and measured points at each fillet sample using fiber probe.

Chemical analysis

Fig. 3.2.2 shown the chemical analysis procedure. After obtaining the fluorescence spectra of all frozen fillet samples, the cylindrical subsamples were cut from the EEM acquired positions of the frozen fillet (3.2.1) for the analysis of ATP-related compounds. The muscle extraction was performed according to Ehira and Uchiyama, 1986 [46]. The dissecting of subsamples was accomplished inside a cold room (4.5 °C), and the frozen fillets and cutting tools were kept cool using dry ice. The solution was frozen and stored at −60 °C until the HPLC analysis.

A rotary saw was used for the sub-sampling and then the skin and red muscles were removed before crushing the excised muscle using a knife, chisel and hammer. The dissecting of subsamples was accomplished inside a cold room (4.5 °C), and the frozen fillets and cutting tools were kept cool using dry ice. The crushed frozen muscle, which weighed around 5 g, was soaked in 15 ml of 10 % perchloric acid (Wako Pure Chemical Industries Ltd., Japan) solution immediately, then homogenized using a rotary homogenizer (Model PT 10-35 GT; Kinematica AG, Lucerne, Switzerland). The whole homogenate was centrifuged (Suprema 21; Tomy Seiko Co. Ltd., Japan) at 2 000×g for 3 min at 4 °C. Subsequently, the supernatant was collected and 5 % perchloric acid was added to the precipitate, and then mixed and centrifuged again three times. Then, the pH adjustment (6.4) was performed using potassium hydroxide. Lastly, the supernatant was diluted with

ion exchange water in a 50 mL volumetric flask, and then the solution was frozen and stored at −60 °C until the HPLC analysis.

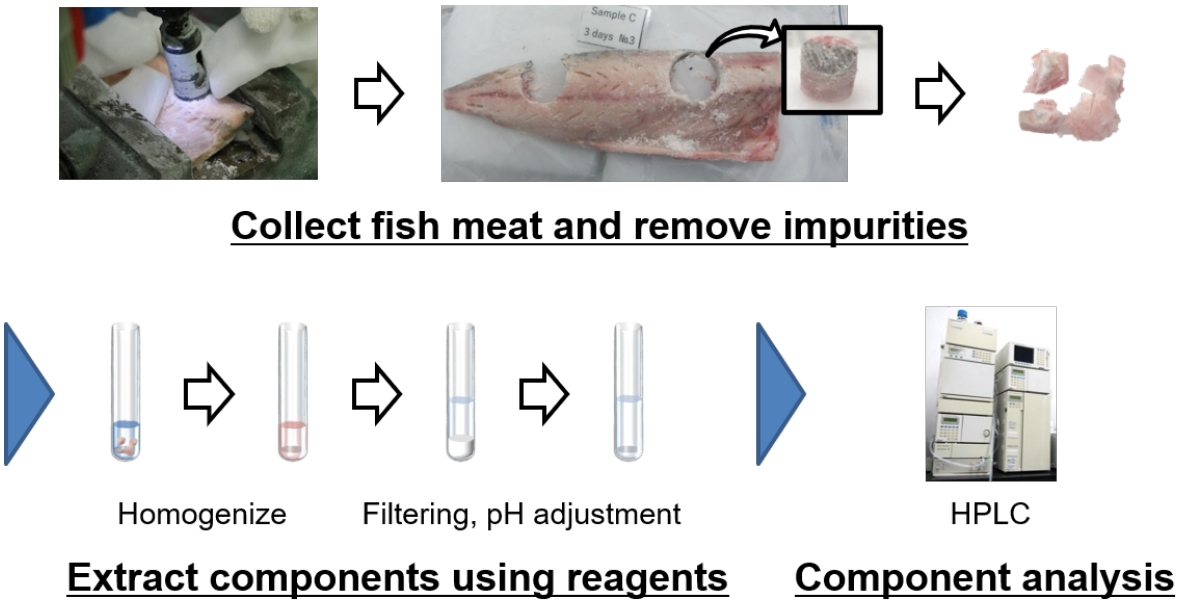

Fig. 3.2.2: Procedure of chemical analysis.

According to Maeda et al. [47], ATP, ADP, AMP, IMP, HxR and Hx in the muscle extracts of frozen fillets were determined using a high-performance liquid chromatography (HPLC) system. Firstly, the supernatants containing muscle extract were thawed at 4 °C and the solutions were passed through a 0.45 µm syringe membrane filter. Next, a solution of 5 µl was injected into the HPLC (LC-10 series; Shimadzu Corp.). For separation of the individual compounds, a stainless-steel column (15 cm × 4.6 mm internal diameter, Shodex C18M4D; Showa Denko K.K., Japan) was used. A buffer of pH 6.8 of 0.13 M triethylamine, 0.20 M acetonitrile, and 0.13 M phosphoric acid (Kokusan Chemical Co., Ltd., Japan) was used as the mobile phase with a flow rate of 0.8 ml/min, at 35 °C. The UV adsorption of the eluent was monitored at 260 nm. The known concentrations of the ATP, ADP, AMP (Oriental Yeast Co. Ltd., Japan), IMP, HxR (Junsei Chemical Co. Ltd., Japan), and Hx (Wako Pure Chemical Inds. Ltd., Japan) standards were injected for calibration of the chromatographic peaks of these compounds. After acquiring the data of all ATP-related compounds from HPLC, the K-value was calculated according to Saito et al. [43] by the following equation:

$$K - value(\%) = \frac{HxR + Hx}{ATP + ADP + AMP + IMP + HxR + Hx} \times 100 \tag{3.1}$$

Fluorescence image measurement

Figure 3.2.3 shows the experimental setup for measuring fluorescence images. In this experiment, the right-side fillets were used for the image measurement. Each frozen fillet sample was placed in the middle of a styrofoam box with dry ice inside to minimize temperature changes of the samples. The temperature inside the styrofoam box was kept under −50 °C. The samples were illuminated by an excitation at 340 nm, which is the most efficient excitation wavelength for freshness prediction of spotted mackerel in a frozen condition (described at 3.3.1), using MAX-303 light source (ASAHI SPECTRA). The fluorescence emitted from the sample was filtered through a band-pass filter to obtain a fluorescence image at a specific emission wavelength. The emission wavelength was controlled by changing the band-pass filter at the filter system. The BU-56DUV CCD camera (Bitran) was used for measuring the fluorescence image at every 10 nm from 380 to 630 nm. The 2×2 binning [48] was used in the measurement with the exposure time set to 1 500 ms for each image. A total of 26 images were measured in each sample. The measured fluorescence images contained dark noise [49, 50] which was corrected by subtracting a dark image acquired by closing the camera shutter and covering the lens with a lens cap so that no light could enter through the lens. The uneven distribution of illuminant was corrected by using images of a spectralon diffuse reflectance target (Labsphere) measured under the same illuminant.

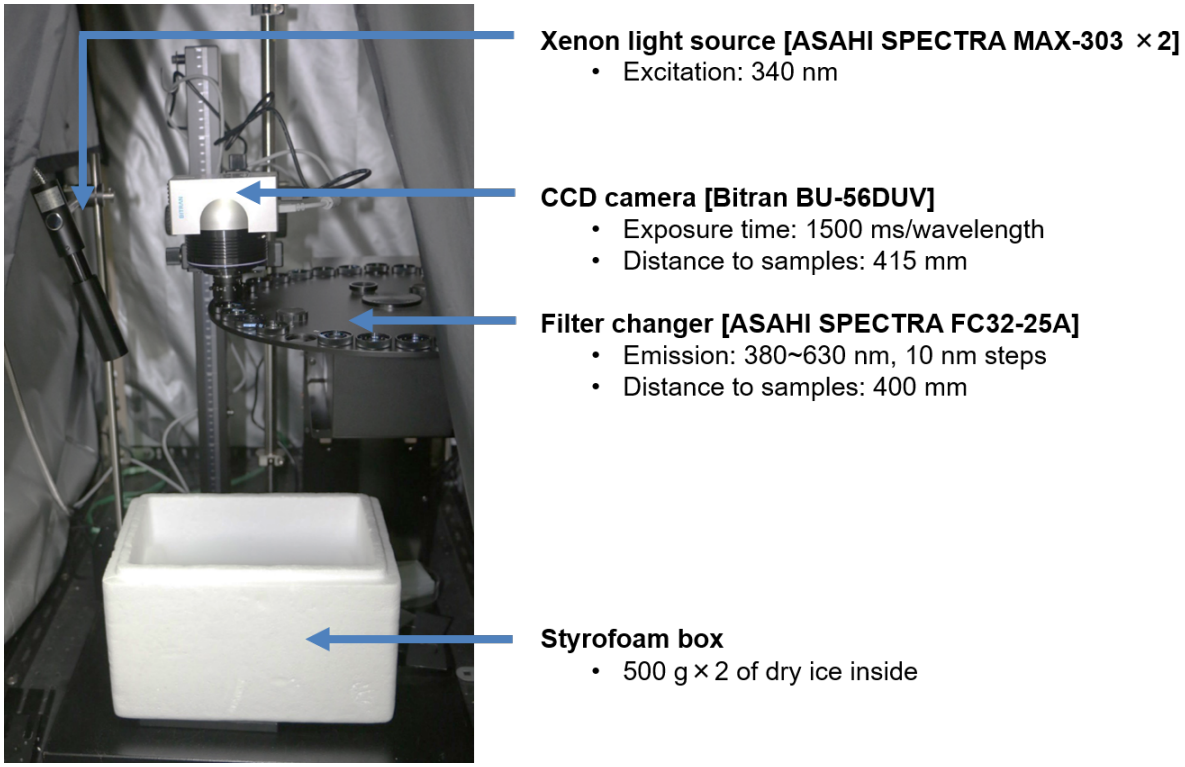

Fig. 3.2.3: Experiment setup for measuring fluorescence images of the frozen fillet samples.

Camera output with excitation and emission filters

In fluorescence fingerprint imaging, the excitation wavelength and emission wavelength are controlled by attaching the band-pass filters to both the light source side (excitation) and the camera side (emission). This section describes a model that represents the camera output when using the narrow band-pass filters. The filter used in the imaging process is assumed to be an ideal band-pass filter, where the transmittance other than the wavelength to be transmitted (single wavelength) is zero. Firstly, the spectrum of illuminant $I'(\lambda_{ex})$ is limited by the excitation filter and is given by:

$$I'(\lambda_{ex}) = I(\lambda_{ex}) \cdot F_{ex}(\lambda_{ex}) \tag{3.2}$$

$$F_{ex}(\lambda_{ex}) \begin{cases} > 0 & \lambda_{ex} = \lambda_i \\ = 0 & \lambda_{ex} \neq \lambda_i \end{cases}$$

where, λ_{ex} is the excitation wavelength, λ_i is the transmission wavelength of the excitation filter, $I(\lambda_{ex})$ is the spectrum of the illuminant before transmitting the excitation filter, $F_{ex}(\lambda_{ex})$ is the transmittance of the excitation filter at λ_{ex}. Then, the spectrum of the object $S(\lambda_{em})$ illumiated by $I'(\lambda_{ex})$ can be described as

follows:

$$S(\lambda_{em}) = I'(\lambda_{ex}) \cdot \{R(\lambda_{ex}, \lambda_{em}) + E(\lambda_{ex}, \lambda_{em})\} \tag{3.3}$$

$$I'(\lambda_{ex}) = \begin{cases} I(\lambda_{ex}) \cdot F_{ex}(\lambda_{ex}) & \lambda_{ex} = \lambda_i \\ 0 & \lambda_{ex} \neq \lambda_i \end{cases}$$

$$R(\lambda_{ex}, \lambda_{em}) = \begin{cases} R(\lambda_{ex}) & \lambda_{ex} = \lambda_{em} \\ 0 & \lambda_{ex} \neq \lambda_{em} \end{cases}$$

where, λ_{em} is the emission wavelength, $R(\lambda_{ex}, \lambda_{em})$ is the reflectance rate, $E(\lambda_{ex}, \lambda_{em})$ is the fluorescence quantum yield. The fluorescence quantum yield is the number of photons at the emission wavelength relative to the number of photons absorbed by the sample at the excitation wavelength and indicates the conversion efficiency between excitation light and emission light (fluorescence). Since the reflected light is much stronger than the fluorescence, λ_{em} is adjusted to be larger than λ_{ex} during the measurement. Therefore, $S(\lambda_{em})$ can be transformed as follow:

$$S(\lambda_{em}) = I'(\lambda_{ex}) \cdot E(\lambda_{ex}, \lambda_{em}) \tag{3.4}$$

From these equations the output of camera with the excitation and emission filters $O(\lambda_{ex,em})$ is given as follows:

$$O(\lambda_{em}) = S(\lambda_{em}) \cdot F_{em}(\lambda_{em}) \cdot C(\lambda_{em}) \tag{3.5}$$

$$F_{em}(\lambda_{em}) \begin{cases} > 0 & \lambda_{em} = \lambda'_i \\ = 0 & \lambda_{em} \neq \lambda'_i \end{cases}$$

where, λ'_i is the transmission wavelength of the emission filter, $F_{em}(\lambda_{em})$ is the transmittance of the emission filter, and $C(\lambda_{em})$ is the camera sensitivity. Therefore, from (3.4) and (3.5), the camera output $O(\lambda_{ex,em})$ through the excitation and emission filters can be transformed as follow:

$$O(\lambda_{ex,em}) = I(\lambda_{ex}) \cdot F_{ex}(\lambda_{ex}) \cdot E(\lambda_{ex}, \lambda_{em}) \cdot F_{em}(\lambda_{em}) \cdot C(\lambda_{em}) \tag{3.6}$$

In (3.6), $E(\lambda_{ex}, \lambda_{em})$ represents the fluorescence properties of the sample. While $I(\lambda_{ex}) \cdot F_{ex}(\lambda_{ex})$ depends on the equipment properties on the excitation side and $F_{em}(\lambda_{em}) \cdot C(\lambda_{em})$ depends on the equipment properties on the excitation side.

Excitation and emission calibration

In order to measure the device-independence fluorescence image, excitation calibration and emission calibration are required. This part shows the method for excitation calibration and emission calibration.

For excitation calibration, the spectral distribution of the random illuminant with excitation filter I' was measured using a spectralon diffuse reflectance target (Labsphere) and a spectroradiometer SR-3AR (TOPCON). The spectral distribution obtained by the spectroradiometer can be given as (3.2). The excitation calibration function can be obtained as follows:

$$N_{ex}(\lambda_{ex}) = \frac{1}{I(\lambda_{ex}) \cdot F_{ex}(\lambda_{ex})} \tag{3.7}$$

For emission calibration, the spectral distribution of the random illuminant L was measured using a spectralon diffuse reflectance target (Labsphere), a spectroradiometer SR-3AR (TOPCON) and BU-56DUV CCD camera (Bitran). The spectral distribution obtained by the spectroradiometer $S_{sd}(\lambda)$ is given by (3.8). The spectral distribution obtained by the camera $S_c(\lambda_{em})$ is affected by the transmittance of the fluorescence filter $F_{em}(\lambda_{em})$, and the sensitivity of the camera $C(\lambda_{em})$, resulting in (3.9).

$$S_{sd}(\lambda_{em}) = I(\lambda_{em}) \tag{3.8}$$

$$S_c(\lambda_{em}) = I(\lambda_{em}) \cdot F_{em}(\lambda_{em}) \cdot C(\lambda_{em}) \tag{3.9}$$

From (3.8) and (3.9), the calibration function for the filter transmittance and camera sensitivity $N(\lambda_{em})$ can be obtained as follows:

$$N_{em}(\lambda_{em}) = \frac{S_{sd}(\lambda_{em})}{S_c(\lambda_{em})} = \frac{1}{F_{em}(\lambda_{em}) \cdot C(\lambda_{em})} \tag{3.10}$$

In this study, the excitation side is illuminated by a single-wavelength light source with a narrow band-pass filter. Therefore, the camera outputs are only affected by the transmittance of the fluorescence filter $F_{em}(\lambda_{em})$ and the camera sensitivity $C(\lambda_{em})$. Thus, only emission calibration was applied.

3.2.2 Experiment 2

Fish samples

In Experiment 2, two groups of spotted mackerel samples harvested from the same fish cage (Kamaishi City, Iwate Prefecture, Japan) were prepared. For the first group, normal meat was prepared using the same procedure (neck breaking) as in Experiment 1. For the second group, fish samples were killed by struggle in air for 30 min to create the burn meat. All fish samples were stored in iced water at 0 °C for 2, 4, 24, 40 h to stimulate the different freshness conditions, then filleted, vacuum packed and frozen by air blast freezer at −60 °C. There were three neck break fish samples and two struggle fish sampless for each condition. The average weight of samples was 349.7±84.9 g and the length of samples was 32.6±2.1 cm

Fluorescence image measurement

The fluorescence images of each samples were measured and calibrated with the same condition as in experiment 1. The samples were illuminated by an excitation at 340 nm. The fluorescence emitted from the sample was filtered through a band-pass filter to obtain a fluorescence image at every 10 nm from 380 to 630 nm.

3.3 Results and discussion

3.3.1 Experiment 1

EEM preprocessing and analysis for predicting the fish freshness

Figure 3.3.1(a) shows the EEM spectra obtained from the fish fillet measurement. The EEM was formed by recording fluorescence intensities at an emission wavelength range of 250~800 nm under the same excitation wavelength range of 250~800 nm. The raw data of EEM includes some parts that do not contain a fluorescence property. There is hypothetically no emission below the excitation based on Stokes' shift [51]. Besides, owing to light scattering effects such as the Raman and Rayleigh effects, a typical scattering problem normally exists in any excitation-emission matrix [52, 53]. Scattering signals and those areas whose emission wavelengths are shorter than the excitation wavelengths do not carry relevant chemical information and should be entirely excluded from the EEM before commencing the building of the calibration models. The preprocessed EEM spectra masked only the fluorescence area after removing those irrelevant areas is shown in Fig. 3.3.1(b).

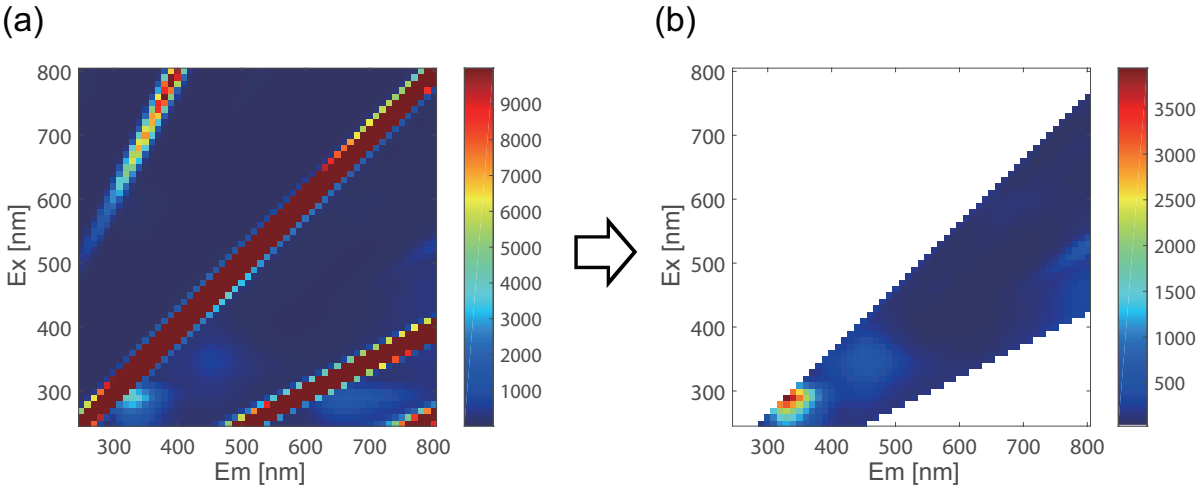

Fig. 3.3.1: EEM preprocessing to remove areas that contains emission wavelengths shorter than the excitation wavelengths and scattering effect. (a) Raw EEM data obtained from measurement. (b) Result of EEM preprocessing.

After EEM preprocessing (i.e. removed irrelative area), the data size of each EEM was reduced to 1 054 from 3 136 variables (each variable corresponds to one excitation-emission wavelength combination of original spectra). The reduced EEM data (1 054 variables) was used to predict the measured K-value and IMP content by a partial least squares (PLS) regression model. The PLS model was built under a leave-one-out cross-validation that used one sample as the validation and the remaining samples as the training set. The prediction accuracy is compared quantitatively using the coefficient of determination (R^2), standard error of prediction (*SEP*) and latent variable (*LV*). The PLS models revealed that EEM could be used to predict K-value and IMP content with high accuracy ($R^2 = 0.86$ and $R^2 = 0.84$, respectively. This is very similar to the result of ElMasry et al. [15], which used all fluorescence intensity at 1 054 variables to predict K-value, with a prediction accuracy of $R^2 = 0.86$.

Selecting the most efficient excitation wavelength

In the PLS prediction models, we used all fluorescence intensity at 1 054 variables on each EEM as predictors, where each variable corresponds to one excitation-emission wavelength combination. Accordingly, when expanding this prediction model to the image, it is necessary to measure a fluorescence image at 1 054 excitation-emission wavelength combinations for each target, which mean 1 054 images. Therefore, in order to visualize the frozen fish quality expressed as K-value and IMP content more competently, reducing the high dimensionality of EEM data is required.

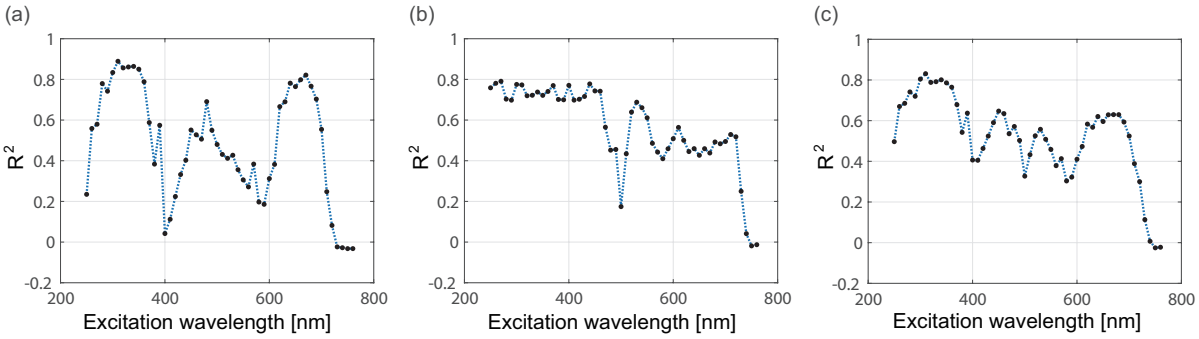

Fig. 3.3.2: Prediction of K-value and IMP content in frozen fish at each excitation wavelength. (a), (b) Repeated PLS regression modeling using all emission wavelengths in the range under each excitation wavelength. (c) Average of (a) and (b).

In this study, the dimension of EEM was reduced by performing repeated PLS regression modeling using all emission wavelengths in the range under each excitation wavelength to identify the most effective excitation wavelength. The results of wavelength selection for K-value and IMP content were shown in Figs. 3.3.2(a) and 3.3.2(b), respectively and average of them in Fig. 3.3.2(c). The prediction accuracy differs for each excitation wavelength and freshness index (K-value and IMP content). In the graph of average accuracy, at the excitation wavelength range of 300~350 nm, the prediction of these freshness indices is lower than those of all 1 054 variables though accuracy is still high (R^2 is more than 0.79). The highest prediction accuracy is at an excitation wavelength of 310 nm ($R^2 = 0.83$) and the next highest prediction accuracy is at an excitation wavelength of 340 nm ($R^2 = 0.80$).

Due to the limitations of the equipment used in the experiment, there is no spectroradiometer that can measure whole emission wavelength (350~570 nm) under an excitation wavelength of 310 nm. For this reason, 340 nm was chosen as the most efficient excitation wavelength instead of 310 nm to visualize fish freshness. Note that, the prediction accuracy under 340 nm is almost equivalent to 310 nm.

Emission calibration and illuminant unevenness calibration

Figure 3.3.3 shows the example of illuminant unevenness calibration. Figure 3.3.4 shows the calibration function for emission filters and BU-56DUV CCD camera (Bitran), which was used for measuring fluorescence images. In order to get the device-indepenent fluorescence images, illuminant unevenness calibration and emission calibration function was used to calibrate the fluorescence images obtained from measurement.

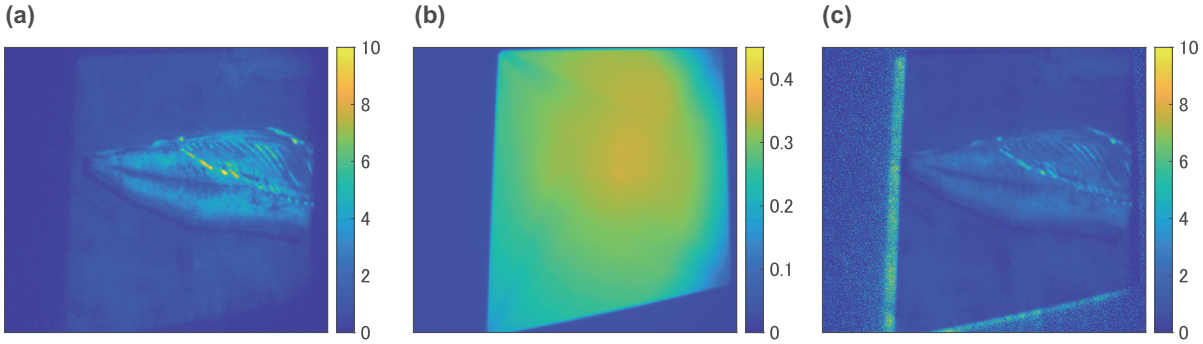

Fig. 3.3.3: Illuminant unevenness calibration. (a) Measured fluorescence image. (b) Illuminant distribution. (c) Calibrated fluorescence image.

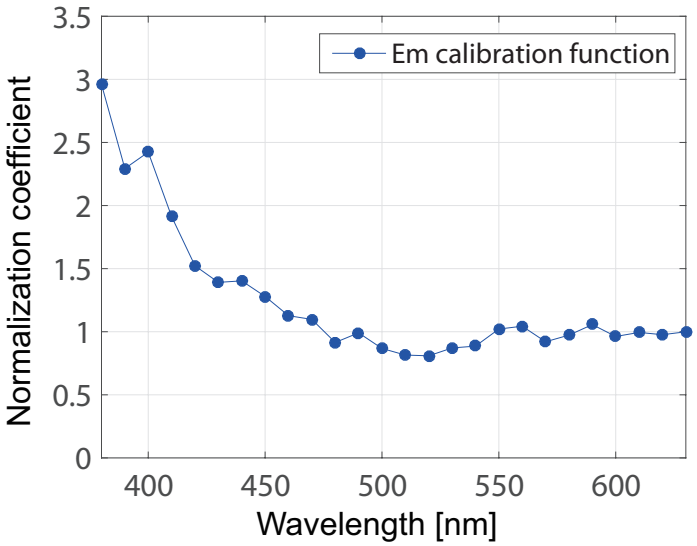

Fig. 3.3.4: Calibration function for emission filters and BU-56DUV CCD camera (Bitran).

Visualization of the quality of frozen fish

In samples preparation (see Section 3.2.1), the fish samples were filleted after being stored in a refrigerator for a specific period, just before being vacuum packed and frozen in a freezer. Thus, in this study, we assumed that the freshness (K-value and IMP content) of the left-side fillets are the same as the freshness of the right-side fillets at the corresponding point.

In order to visualize the frozen fish freshness expressed by K-value and IMP content, we need to build a prediction model from the measured fluorescence images. The areas corresponded to the fluorescence measurement and the chemical analysis (Fig. 3.2.1) were used for analysis. For each fluorescence image, those areas were masked and the pixels value inside the mask was averaged. There were 26 fluorescence images, yielding 26 variables obtained for each point. In this study, we have 24 fish samples and two points were measured for EEM for each fish sample, consequently 26 variables at 48 points were obtained. Those 26 variables were used for predicting the K-value and IMP content at corresponding points by PLS regression model. The PLS model was built utilizing leave-one-out cross-validation which used data at one point as the validation and the remaining points as the training set. The prediction accuracy is evaluated by using the coefficient of determination (R^2) and standard error of prediction (SEP).

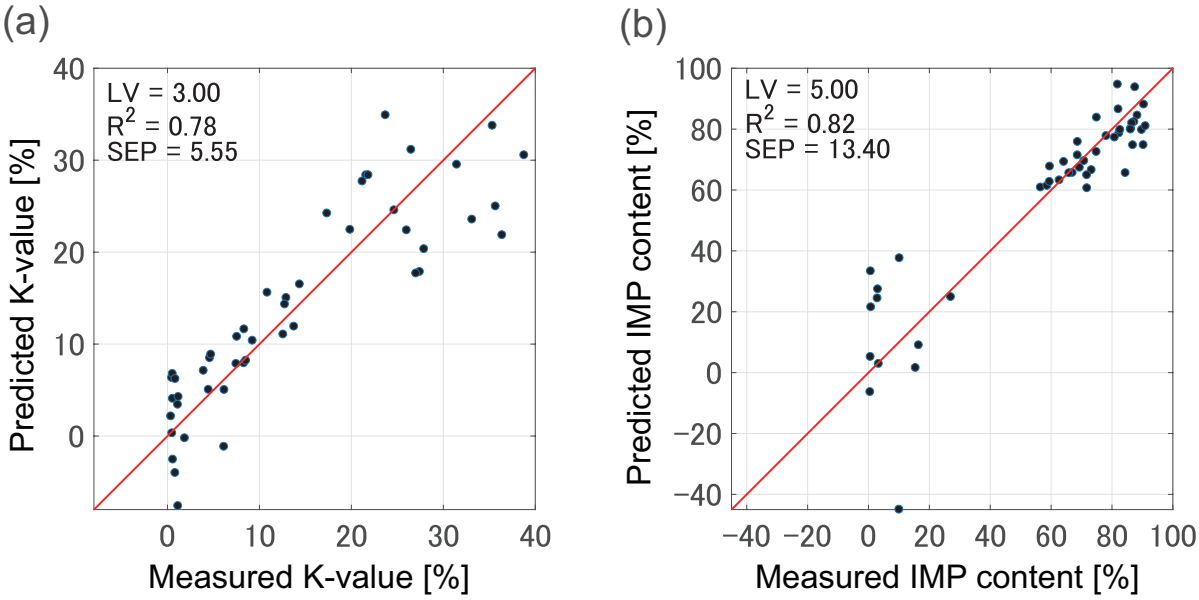

Fig. 3.3.5: Prediction of K-value (a) and IMP content (b) by PLS regression models using all 26 fluorescence images.

Fig. 3.3.5 shows the result of predicting K-value and IMP content (measured in the left-side fillets) at EEM measurement points (Fig. 3.2.1) by using fluorescence images. The prediction accuracy of the PLS models from the measured fluorescence images were $R^2 = 0.78$ for K-value and $R^2 = 0.82$ for IMP content. These are lower than those prediction models using all 1 054 variables of EEM ($R^2 = 0.86$ for K-value and $R^2 = 0.84$ for IMP content). However, the aim of the visualization is to make visible the spatial-temporal freshness changes of a whole sample with acceptable accuracy. Thus, the prediction accuracy of these PLS models ($R^2 = 0.78$ for K-value and $R^2 = 0.82$ for IMP content) is high enough and are acceptable for the visualization.

From the obtained prediction models, the distributions of K-value and IMP content can be estimated by combining the parameters of the prediction models with fluorescence image at corresponding emission wavelength to obtain the freshness distribution image as follows:

$$y_n = \beta_{380} x_{n\,380} + \beta_{390} x_{n\,390} + \cdots + \beta_{630} x_{n\,630} + \beta_0 \tag{3.11}$$

where n is the sample number, β is the parameters of the prediction model, x is the fluorescence image of sample n at specific emission wavelength measured at Section 3.2.1. The result of the visualization of the distributions of K-value and IMP content are shown in Fig. 3.3.6 and Fig. 3.3.7. There were three samples for each storage time condition. The samples in Fig. 3.3.6 are same as samples in Fig. 3.3.7, which are result

of visualize K-value and IMP content, respectively. As a result, K-value increased in accordance with ice storage time. On the other hand, IMP content rapidly increased for the storage period from 0 to 1 day, and then gradually decreased from 2 to 9 days.

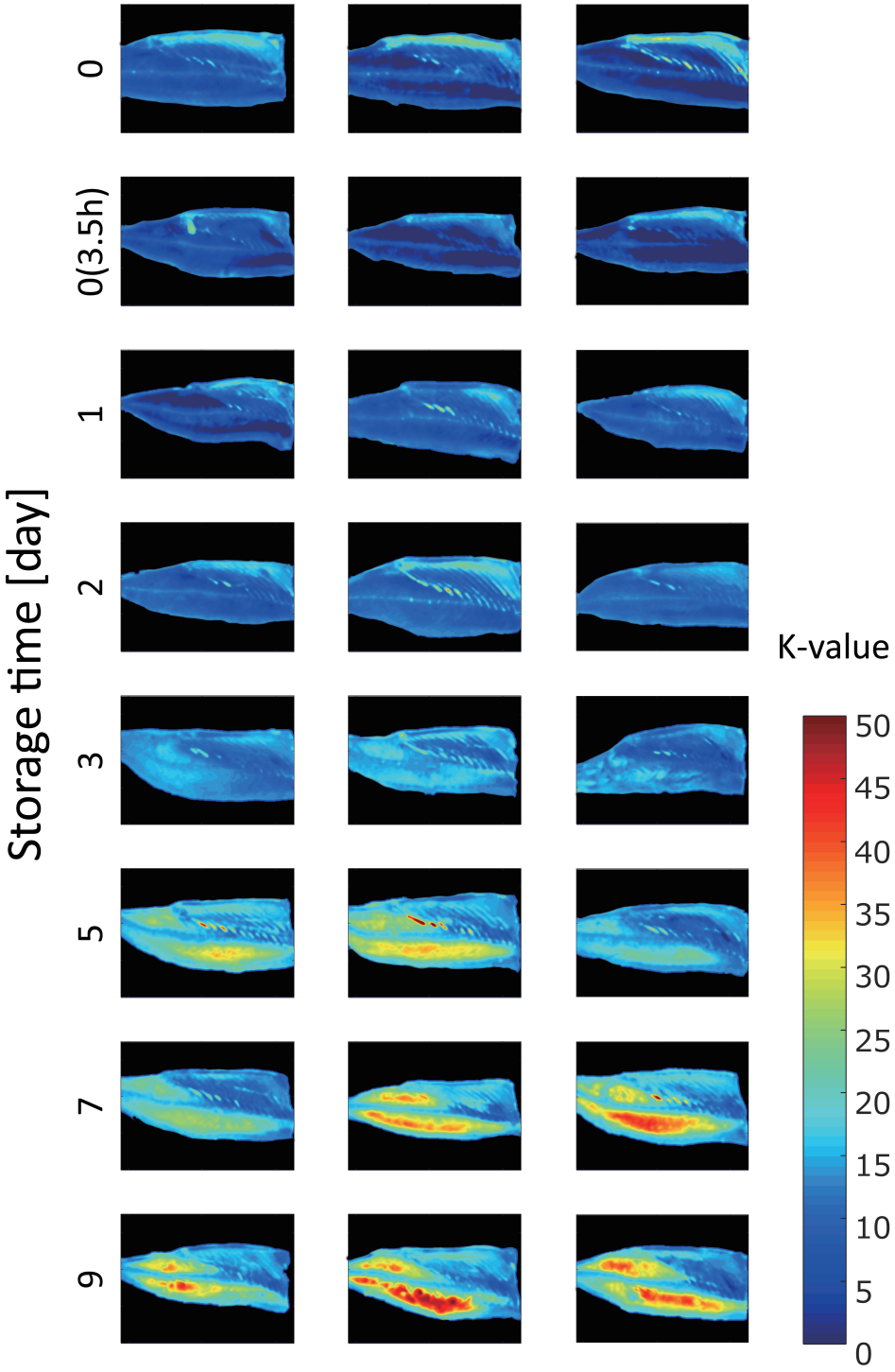

Fig. 3.3.6: Visualization of the spatial-temporal changes of K-value in frozen fish fillets.

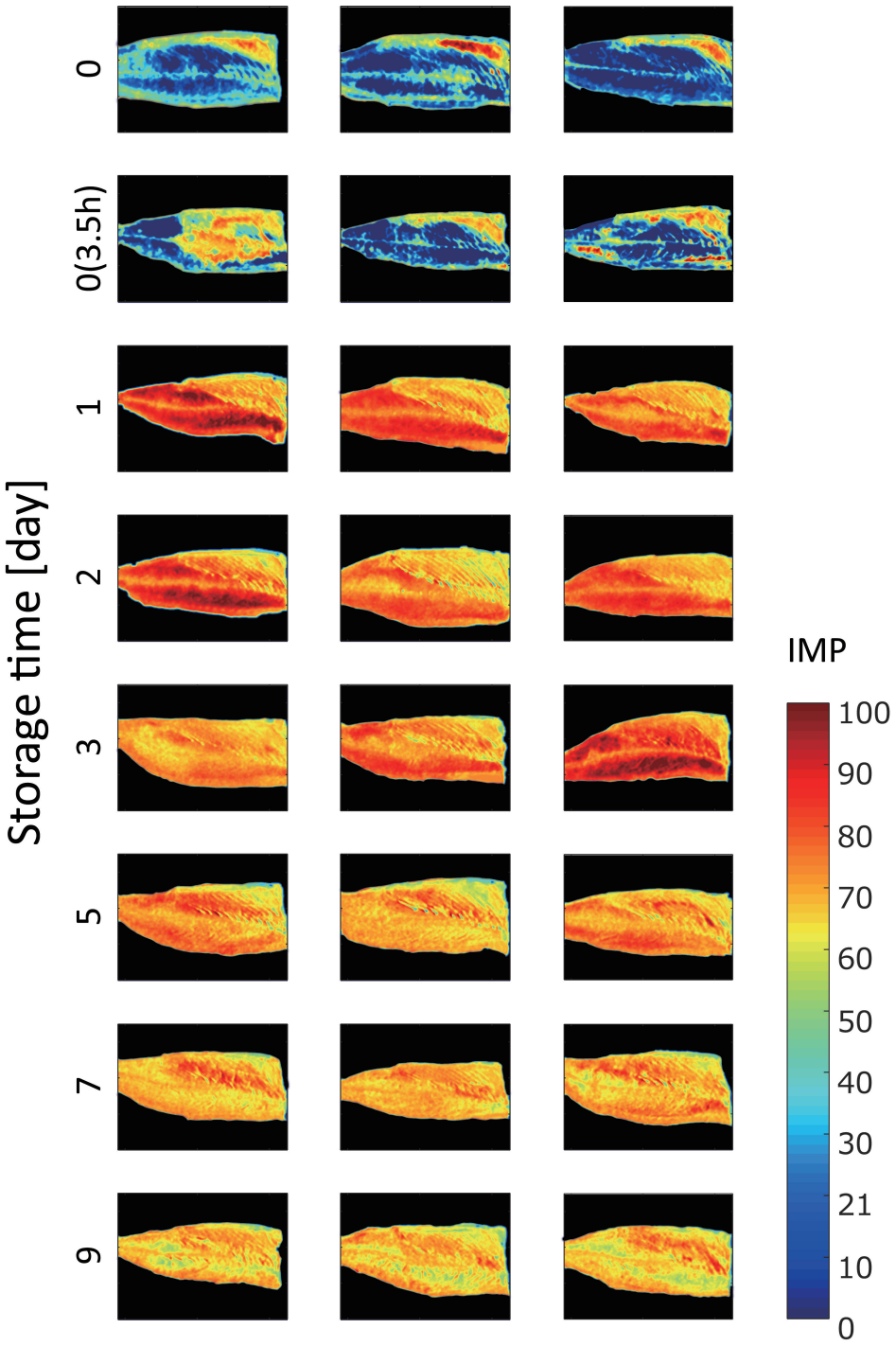

Fig. 3.3.7: Visualization of the spatial-temporal changes of IMP content in frozen fish fillets.

The measured K-value and IMP content obtained from chemical analysis are shown in Figs. 3.3.8(a) and Fig. 3.3.8(c), respectively. As a result, K-value increased linearly with storage time. On the other hand, IMP content increased dramatically from 0 % to 90 % for the samples from 0 to 1 day, and then gradually decreased for the samples from 2 to 9 days. From the visualization result obtained in Fig. 3.3.6 and Fig. 3.3.7, the average of estimated K-value and IMP content in each of the fish samples were calculated. The estimated K-value and IMP content are shown in Figs. 3.3.8(b) and 3.3.8(d), respectively. As expected, the changes of K-value and IMP content obtained from chemical analysis and estimated from fluorescence images showed the same trend and as same as the previous studies [43, 54, 55], ATP inside the muscle is decomposed rapidly. After the decomposition of ATP, ADP and AMP are also decomposed quickly and advance to IMP in a stroke, occur instantaneous accumulation of IMP. Furthermore, IMP thus formed is slowly converted to HxR and then to Hx, which means the slowly increasing of K-value. The comparison of measured and estimated K-value and IMP content obtained from chemical analysis at three parts (back, belly, tail) are shown in Fig. 3.3.9. The change in both K-value and IMP content differ for each part of the fish. The back part and tail part, which were used for chemical analysis, showed the highest K-value compared to other parts. Therefore, the average of estimated K-value and IMP content change is slightly smoother than the measured value, which was point measurement.

This result suggested that the purposed method could accurately visualize the distribution of both K-value and IMP content using only one excitation light and be practical for large-scale commercial purposes with a vast number of fish or large fish such as tuna.

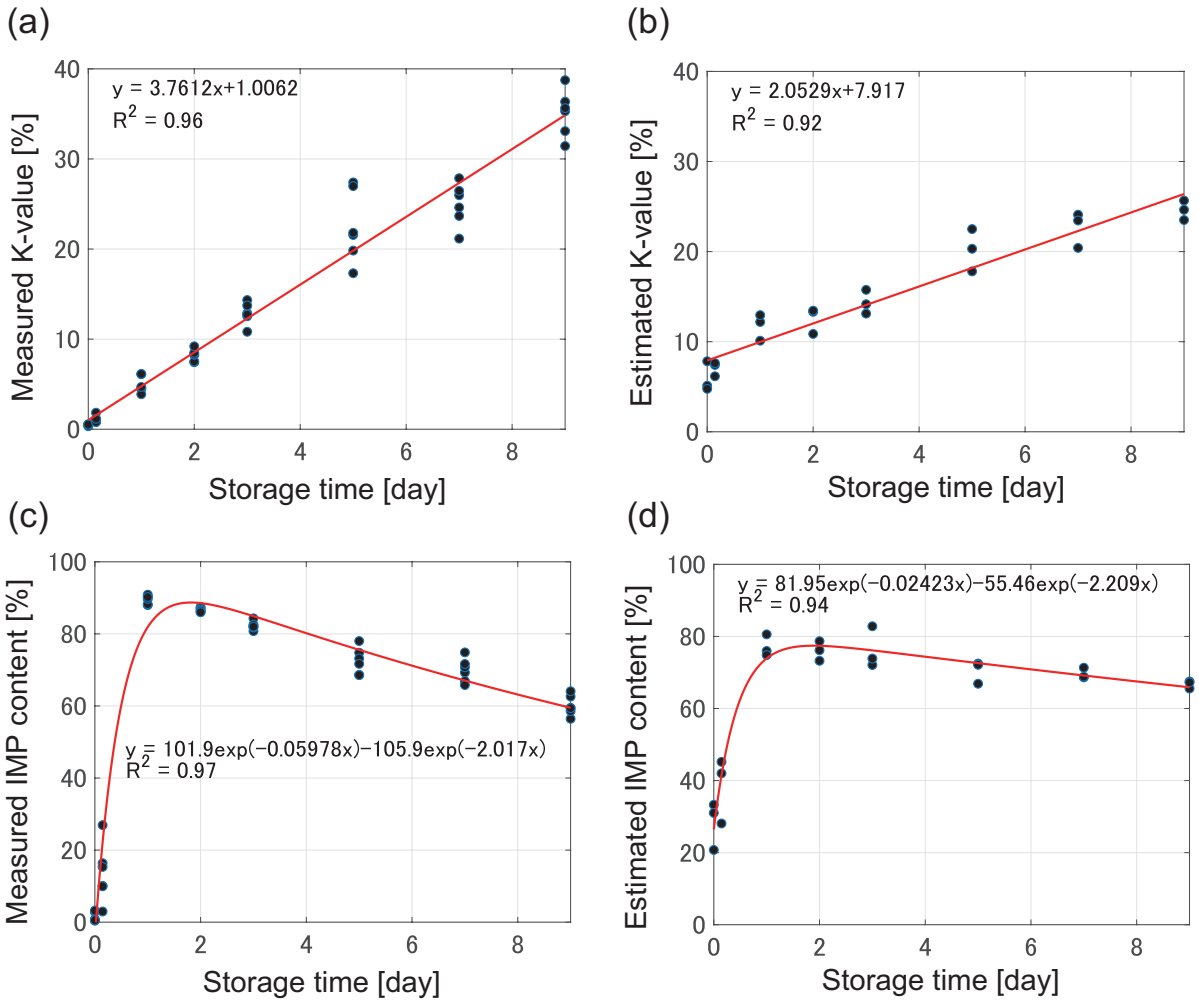

Fig. 3.3.8: Comparison of measured and estimated values of K-values and IMP content. (a) (c) The measured *K*-value, IMP content obtained from chemical analysis. (b) (d) The estimated *K*-value, IMP content calculated by averaging the distribution images obtained in Fig. 3.3.6 and Fig. 3.3.7, respectively.

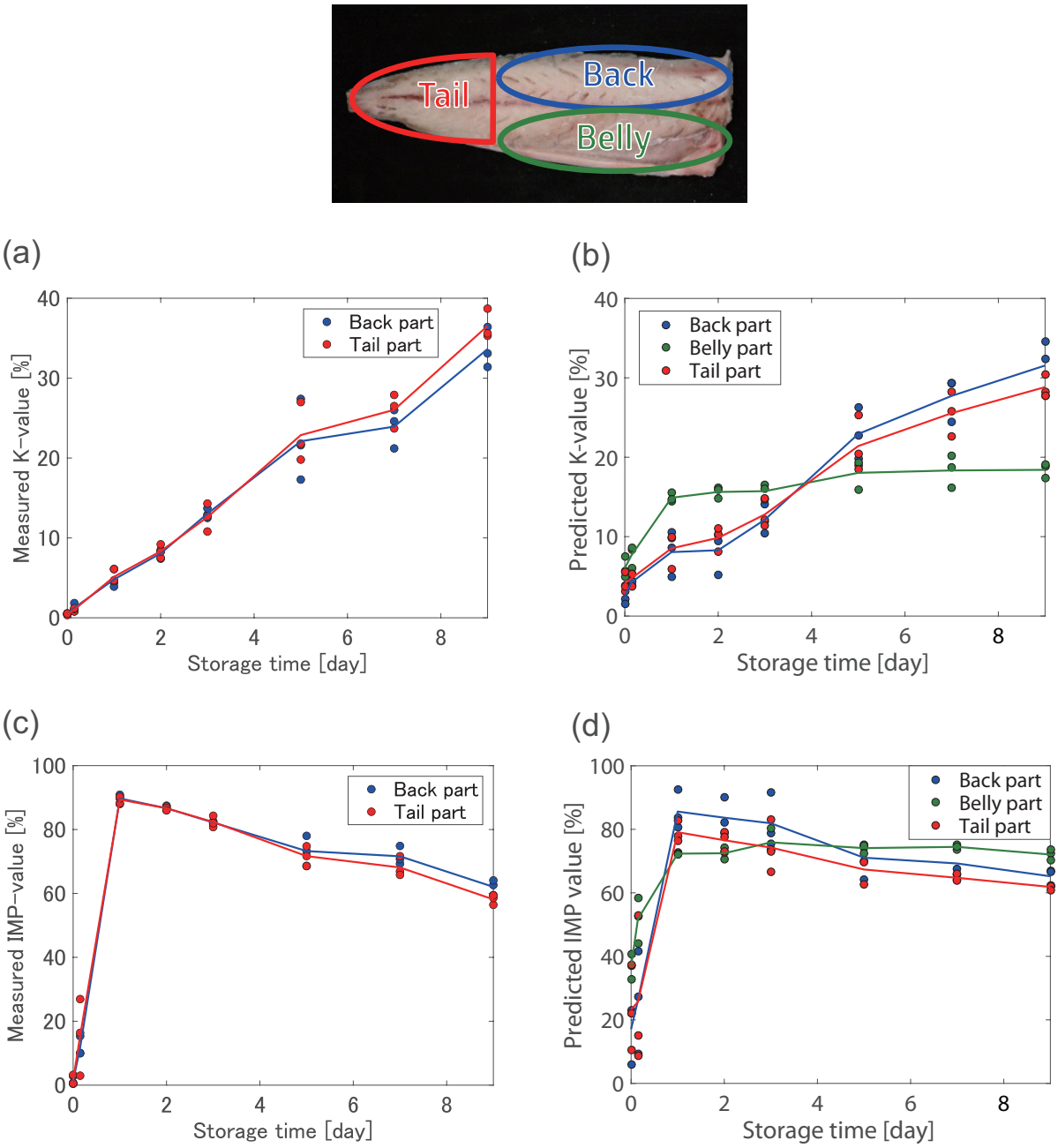

Fig. 3.3.9: Comparison of measured and estimated K-values and IMP content at different parts. (a) (c) The measured K-value, IMP content at three parts (back, belly, tail) obtained from chemical analysis. (b) (d) The estimated K-value, IMP content at three parts (back, belly, tail) calculated by averaging the distribution images obtained in Fig. 3.3.6 and Fig. 3.3.7, respectively.

3.3.2 Experiment 2

Figure 3.3.10 and Figure 3.3.11 shows the K-value distributions of the neck break sample and struggle sample, respectively. As expected, the changing of K-value in the struggle samples is different compared to the neck break samples (instantly killed). Concretely, the K-value of the struggle samples is much higher for meat around the backbone compared to the neck break samples. In general, while the fish is struggling, muscles around the backbone move more intensely. For this reason, meat around the backbone tends to be burnt meat and the K-value is considered to be increased faster [56].

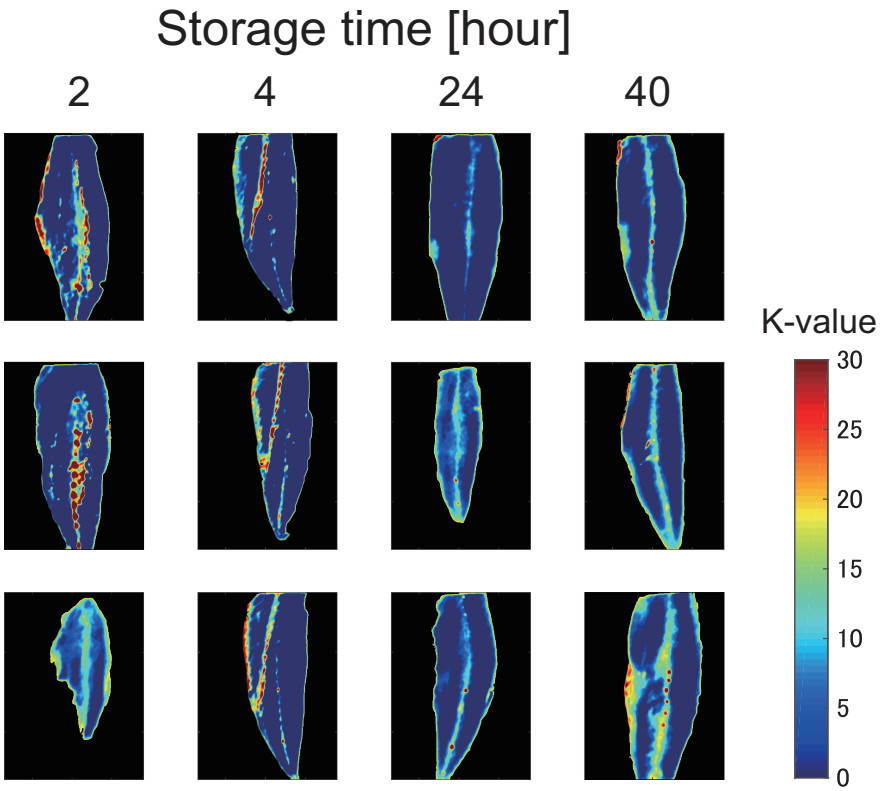

Fig. 3.3.10: Visualization of the K-value distributions of the struggle samples by applying the visualization models obtained in experiment 1.

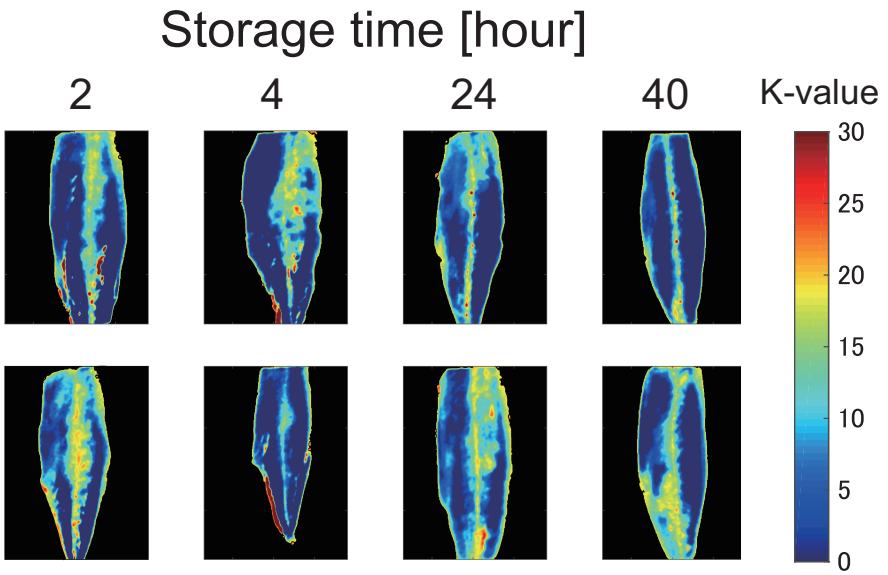

Fig. 3.3.11: Visualization of the K-value distributions of the struggle samples by applying the visualization models obtained in experiment 1.

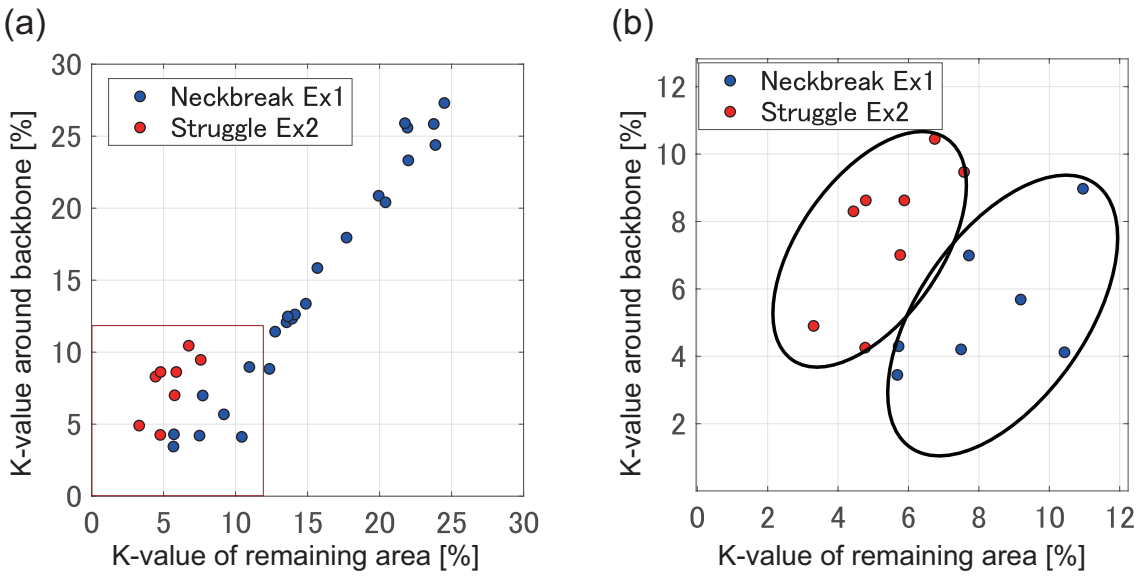

Fig. 3.3.12: (a) Comparison of K-value of the neck break samples in experiment 1 and the struggle samples in experiment 2. Vertical axis is average of K-value in area around backbone, while horizontal axis is average of K-value of remaining area. (b) Zoom in on the samples have almost the same K-value.

Figure 3.3.12(a) shows the average of K-value in area around the backbone and remaining area. As a result, from the average K-value of the area around the backbone and the average K-value of the remaining area, Fig. 3.3.12(b) shows the zoom in on the neck break samples and the struggle samples, which have almost the same K-value. As expected, the neck break samples and the struggle samples can be divided into two groups. It is suggested that burnt meat could be detected even in frozen condition by visualizing the distributions of K-value. As the freshness condition of frozen fish meat cannot be tracked without thawing the sample, this visualization method could be a promising tool to solve the problem.

Chapter 4

Versatile band-pass filters for fluorescence imaging

4.1 Introduction

In order to estimate the chemical properties of the target, the previous studies fixing the excitation at a specific wavelength [17, 18, 57], or using specific excitation-emission combinations [13, 23, 58], or using the ratio of fluorescence intensity at two specific excitation-emission combinations [59, 60] instead of using the whole data of EEM. Furthermore, hyperspectral imaging was applied under multiple excitation-emission combinations in order to visualize the distribution of target property instead of the point estimation [61, 62]. The determination of a chemical property or the classification of geographical origin of food can be carried out with high accuracy using EEM. However, adopting fluorescence as a technique for determining the quality and authenticating food products is still limited, as different wavelengths are chosen for different estimation targets in the calibration stage. Therefore, different band-pass filters are needed for different estimation targets, making it a costly technique. This study proposes the versatile band-pass filters for fluorescence imaging of the food product for quality assessment, which is expected to estimate or classify different targets by using one system. For example, the versatile band-pass filters can be applied to the fruit and vegetable sorting system, where required to sort different kinds of fruits and vegetables.

The study is conducted in two phases. In the first phase, we selected 70 compounds related to food nutrition, freshness, and umami components as samples for fluorescence spectra (EEM) measurement. From the obtained EEM, we generated a synthetic EEM dataset for analysis. Parallel factor analysis (PARAFAC) was applied to the generated synthetic EEM dataset in order to define the exaction-emission wavelength of

the band-pass filters. In the second phase, the practicality of the proposed band-pass filters was verified by employing them to solve a real problem.

4.2 Material and methods

4.2.1 Defining new excitation-emission band-pass filters

Sample selection

Molecular structure and chemical environment affect whether or not a substance fluoresces. Generally, the molecules that fluoresce have conjugated systems, which have alternating single and multiple bonds. The food we eat contains many substances; however, not all of them have the conjugated system and emit fluorescence.

In this study, compounds related to food nutrition (e.g., vitamins and essential amino acids), freshness, and umami components were selected as samples for fluorescence spectral measurement. Furthermore, compounds reported in previous studies, such as chlorophyll and ferulic acid, were also selected for the experiments [19, 20, 63]. Moreover, a list of the top 100 compounds in food was compiled from FooDB version 1.0, the world's largest and most comprehensive resource on food constituents, chemistry, and biology (www.foodb.ca). Then only compounds with a conjugated system were selected as experiment samples since they have capability to produce fluorescence. In total, 72 compounds were selected as samples for fluorescence spectral measurement. All reagents used in the experiments were of special grade or higher (see Table A.1 - A.3).

Fluorescence spectral measurement (EEM)

For EEM measurement, Milli-Q water, phosphate buffer, ethanol, and acetonitrile were used as solvents. The reagents were dissolved in solvents at concentrations of 0.1, 1, 10, and 100 ppm (1 ppm = 1 mg/L). Then, 300 µL of each dissolved sample was placed into the SQ grade quartz micro cuvette (GL Sciences FM20-SQ-3). EEM was measured using a fluorescence spectrophotometer (F-7000, Hitachi High-Tech Science Corporation) with a right-angle geometry. The cuvette was placed in the spectrophotometer with the shorter path length side facing the excitation light source. The excitation wavelength was changed at 5 mm intervals in the range 200~800 nm, and the emission wavelength was detected at 2 mm intervals in the range 200~800 nm. The slit width on both sides was 5 nm. The photomultiplier voltage was adjusted between 400 and 900 V with a scanning speed of 30 000 nm/min. The solution concentrations and the photomultiplier voltage were

adjusted to acquire an EEM with the lowest signal-to-noise ratio.

EEM preprocessing and generation of the synthetic EEM data

The raw EEM data includes some non-fluorescence components. There is hypothetically no emission below the excitation wavelength based on Stokes' shift. Further, owing to light scattering effects such as Raman and Rayleigh scattering, a wavelength region where fluorescence and scattered light are superimposed typically exists in any EEM [52,53]. Therefore, the scattering signals and areas with emission wavelengths are shorter than the excitation wavelengths do not carry relevant chemical information and were excluded from the EEM.

Based on the detected fluorescence, standard reagents were selected. The EEM for the standard reagents contains the fluorescence spectra of the corresponding compounds. However, food contains a large variety of compounds with overlapping fluorescence spectra. For this reason, in this study, the EEMs for the standard reagents were used to generate synthetic EEM data, which were the random weighted sum of EEMs for the standard reagents with a uniform distribution, and with the sum of the weights normalized to 1. In total, 1 000 synthetic EEM spectra were generated.

Parallel factor analysis

The obtained EEM data is three-way data (excitation, emission, and samples), which provides a large amount of information. Parallel factor analysis (PARAFAC) is a multivariate analysis method originating from psychometrics [64,65]. In contrast to conventional methods such as principal component analysis (PCA), which deals with two-way array data (variable and sample axes), PARAFAC is a method for separating components from multi-way data. In EEM data analysis, PARAFAC separates overlapping fluorescence spectra into individual spectra corresponding to component chemicals in the sample. The results of PARAFAC are a set of scores and loadings, which is the same as for PCA. However, in contrast to PCA, PARAFAC yields two sets of loadings, which are emission loadings and excitation loadings.

A major practical obstacle for using the PARAFAC model is the need to determine the appropriate number of components. The number of components in the PARAFAC model can be obtained from the core consistency diagnostic, which evaluates the 'appropriateness' of the model [66]. The core consistency is always less than or equal to 100 % and may also be negative. A core consistency close to 100 % implies an appropriate model. If a dataset is modeled using PARAFAC with an increasing number of components, the core consistency will typically decrease more or less monotonically and gradually, and then will decrease abruptly

beyond a certain number of components [66].

In practice, for real-world non-ideal datasets, the core consistency is not always a reliable diagnostic for finding the required number of PARAFAC components [67]. Harshman proposed a method called split-half analysis to confirm that a PARAFAC model is appropriate [68]. The split-half analysis examines different subsets of the data independently, and the same result (same loadings) will be obtained in the non-split modes from models of any suitable subset of the data if the correct number of components is chosen. If too few or too many components are chosen, the model parameters will differ if the model is fitted to different datasets.

In this study, PARAFAC and split-half analysis were applied to extract the principle components from the generated EEM dataset. Core consistency and similarity of split-half analysis were used as indicators for determining the appropriate number of components. Savitzky-Golay smoothing [69] along with emission wavelength axis and data normalization, in which the fluorescence intensity at each wavelength is divided by the summed d value of the intensities at all wavelengths (i.e., normalized to have the same multivariate vector length), were applied before the analysis. The PLS_Toolbox v8.8.1 (Eigenvector Inc. Wenatchee, WA, USA) was used for PARAFAC and split-half analysis. Subsequently, the excitation-emission band-pass filters were determined from the principle component loadings.

4.2.2 Verifying the practicality of the proposed band-pass filters

Three EEM datasets related to food from previous studies are used for verification [21, 22, 62]. A summary of the parameters for these datasets is shown in Table 4.2.1. The PLS_Toolbox v8.8.1 was used for the analysis. The analysis methods and calibration vs. validation ratio were the same or as similar as possible to those in previous studies [21, 22, 62]. The 4-filter and 7-filter datasets were calculated by summing the fluorescence intensities of the corresponding wavelength ranges in the original EEM data. Accordingly, four and seven variables corresponding to 4-filter and 7-filter datasets were obtained. Subsequently, four types of preprocessing methods (mean center, autoscale, normalize + mean center, normalize + autoscale) were applied to the filter data, and the one with the best result was selected as the optimum preprocessing method.

Table 4.2.1: Details of datasets from previous studies: Nutmeg, Frozen fish, and Mango.

Dataset	**Nutmeg [21]**	**Frozen fish [62]**	**Mango [22]**
Ex	250~700 nm, 10 nm step	250~800 nm, 10 nm step	200~870 nm, 10 nm step
Em	260~720 nm, 10 nm step	250~800 nm, 10 nm step	230~900 nm, 10 nm step
Sample	calibration 61, validation 30	48	544
Target	aflatoxin contamination	K-value, IMP	geographic origin
Previous method	PLS	PLS	canonical discriminant analysis
Applied method	PLS	PLS	PLSDA

4.3 Results and discussion

4.3.1 Defining new excitation-emission band-pass filters

EEM preprocessing and generation of synthetic EEM data

Of the 70 reagents tested, 41 reagents emitted fluorescence, and two of these (caffeic acid and pyridoxine) emitted fluorescence in two different solvents (see Table A.1 - A.3). Therefore, 43 EEMs showing fluorescence were obtained. Fig. 4.3.1(a) shows the EEM spectra of adenosine 5'-triphosphate (ATP) obtained from fluorescence spectral measurement. The preprocessed EEM spectra masked only the fluorescence area after removing the irrelevant areas as shown in Fig. 4.3.1(b). Those reagents were selected as standard reagents, and the preprocessed EEM spectra were used to generate a synthetic EEM dataset. In total, 1 000 synthetic EEM spectra were generated by synthesizing 43 EEMs for standard reagents with random weights. One representative generated EEM spectra is shown in Fig. 4.3.1(c).

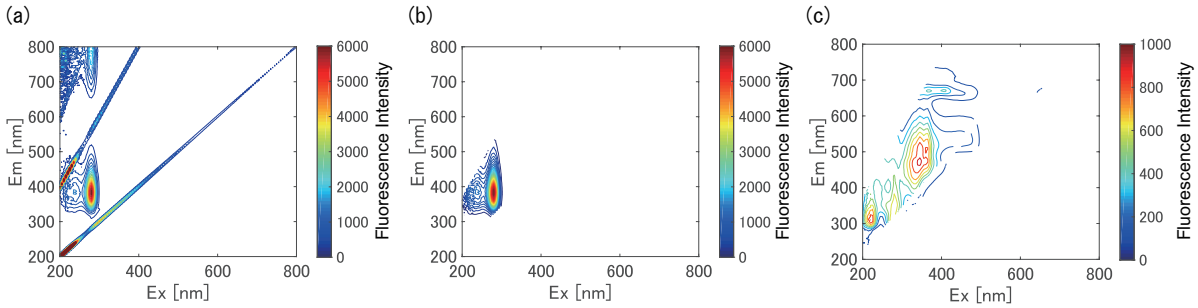

Fig. 4.3.1: EEM preprocessing to remove areas that contains emission wavelengths shorter than the excitation wavelengths and scattering effect. (a) Raw EEM data obtained from measurement. (b) EEM data after preprocessing. (c) Generated synthetic EEM.

PARAFAC

The result of applying PARAFAC on generated synthetic EEM dataset at different component numbers is shown in Fig. 4.3.2(a). In this study, the split-half analysis was also applied to generated synthetic EEM dataset at different component numbers. The result of five times split-half analysis is shown in Fig. 4.3.2(b). In Fig. 4.3.2(a), for one to three number of components, the core consistency was close to 100 %. The core

consistency decreased with increasing the number of components and became negative with a component number of nine and above. This is because the influence of noise and other non-trilinear variation increases with increasing the number of components [66]. In Fig. 4.3.2(b), at the number of components from one to four the similarity of the results (loadings) from the split-half analysis were high. For component number from five to seven, the similarity was high (more than 70 %) depending on the the splitted subsets.

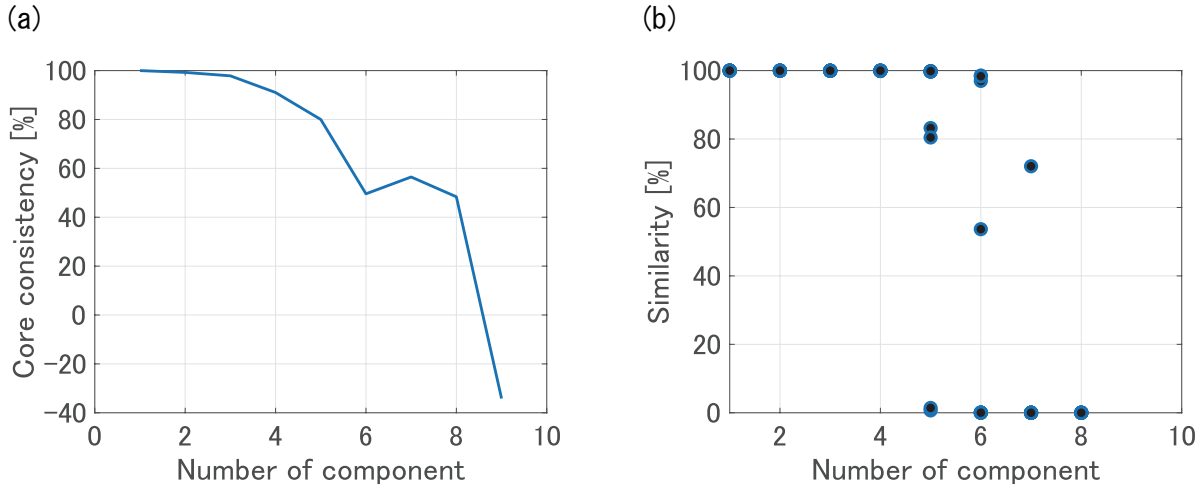

Fig. 4.3.2: Core consistency of PARAFAC model (a), and similarity of five times split-half analysis (b) at different component number.

In this study, PARAFAC and split-half analysis were applied to determine the appropriate number of excitation-emission band-pass filters and not for separating components from generated synthetic EEM dataset. Therefore, four to seven seven were selected as the appropriate number of excitation-emission band-pass filters. PARAFAC at four to seven components were applied on generated synthetic EEM dataset. At each loading obtained from PARAFAC, all possible combinations of excitation-emission wavelengths within the preprocessed range (see Fig. 4.3.1(c)) were calculated. After that, the excitation-emission band is defined as the one with the largest loading sum among them (purple rectangle of Fig 4.3.3 and Fig. 4.3.6). The obtained loadings and defined excitation-emission bands at four components and seven components are shown in Fig. 4.3.3, Fig. 4.3.6, and Table 4.3.1.

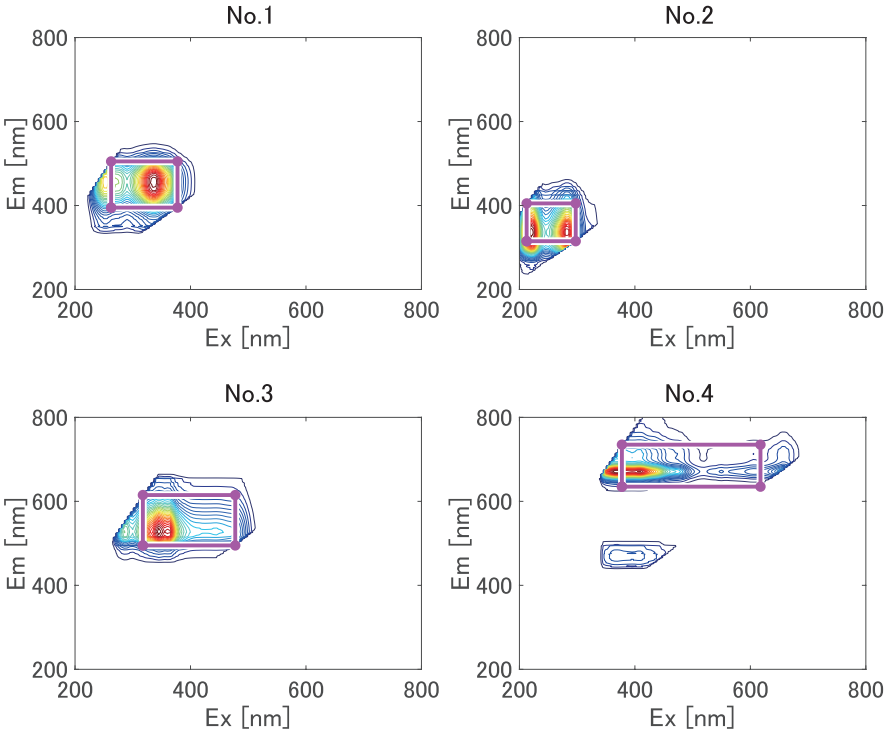

Fig. 4.3.3: Loadings of four components PARAFAC and defined excitation-emission bands of 4-filter (**purple rectangle**).

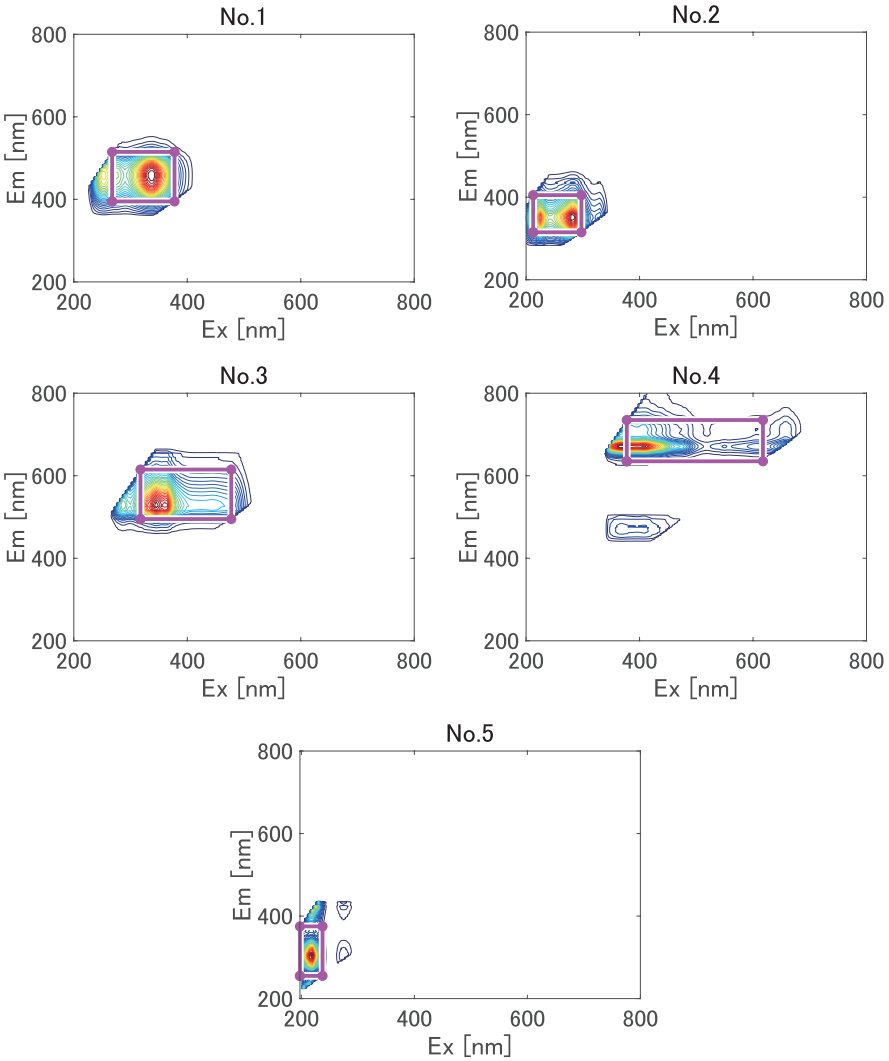

Fig. 4.3.4: Loadings of five components PARAFAC and defined excitation-emission bands of 5-filter (**purple rectangle**).

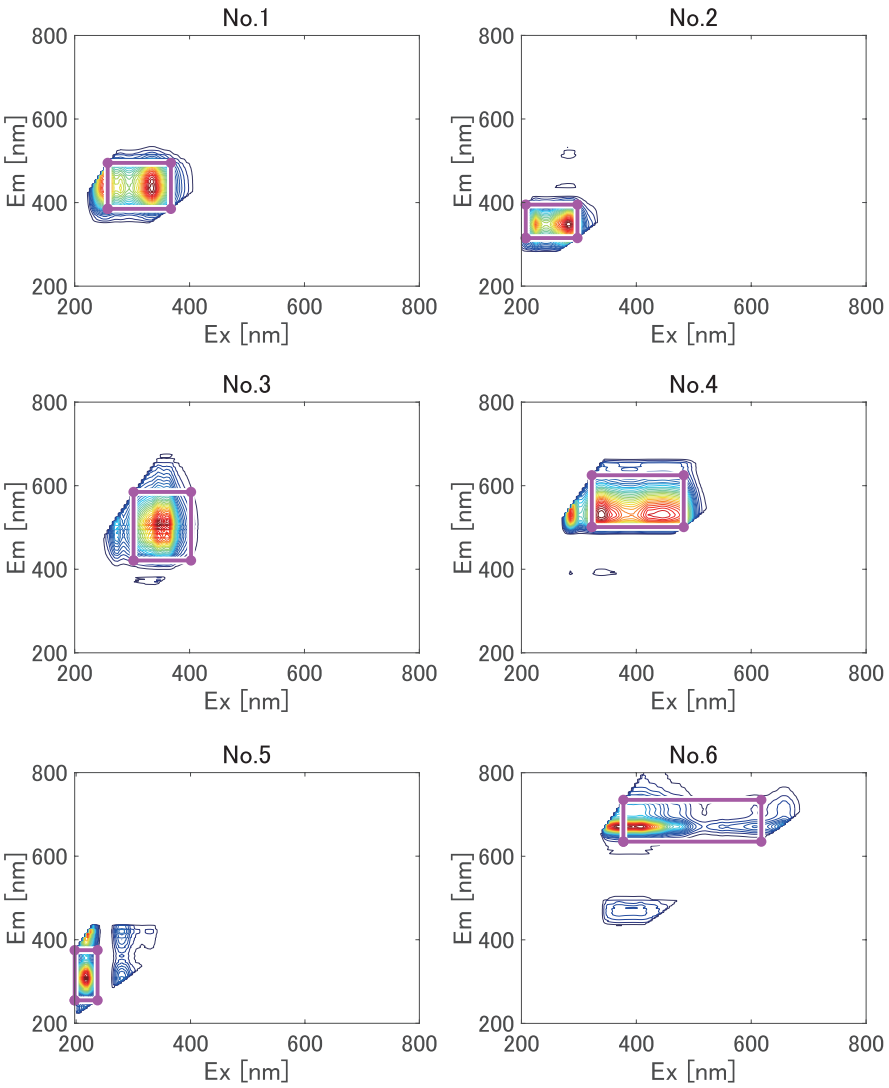

Fig. 4.3.5: Loadings of six components PARAFAC and defined excitation-emission bands of 6-filter (**purple rectangle**).

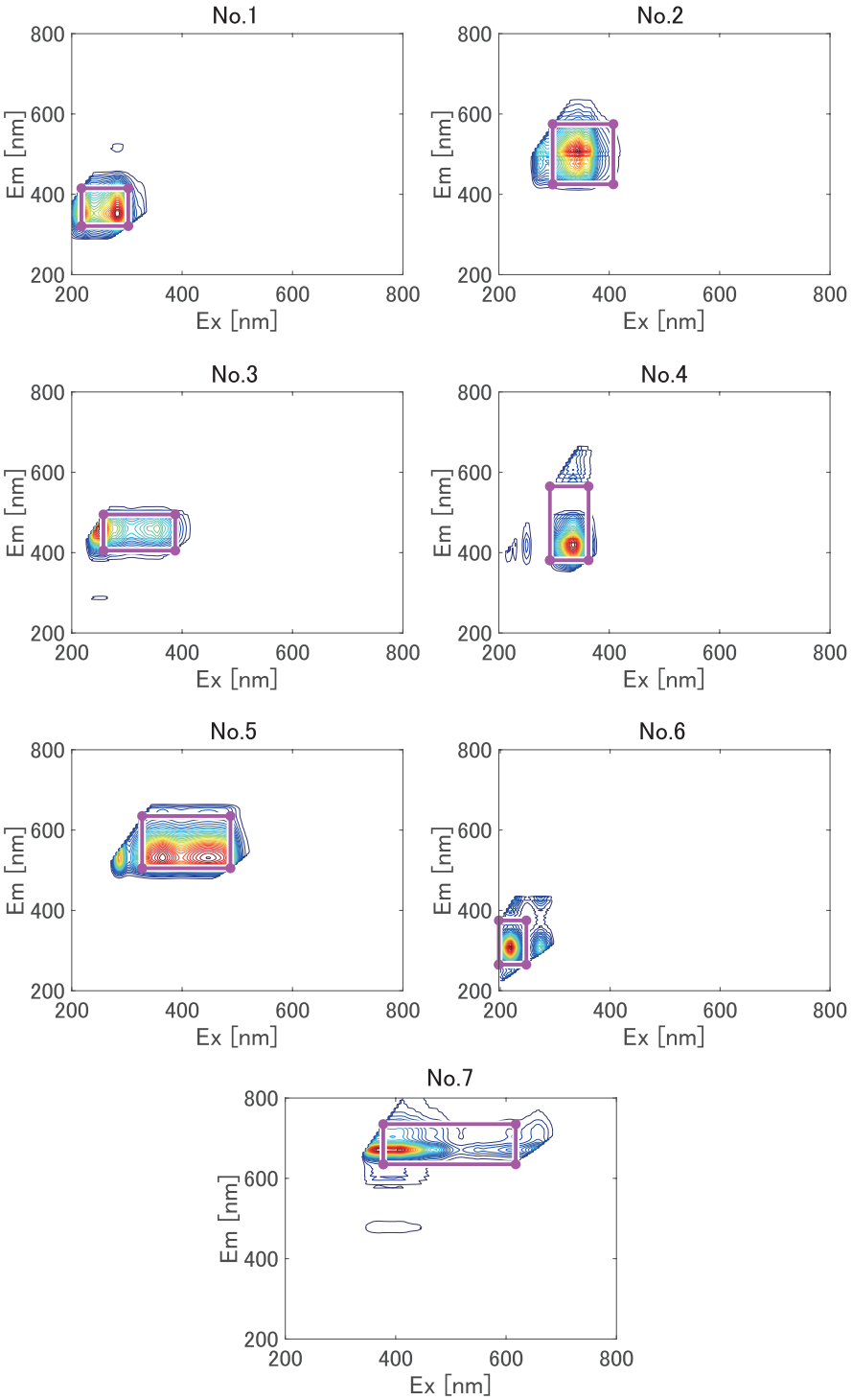

Fig. 4.3.6: Loadings of seven components PARAFAC and defined excitation-emission bands of 7-filter (**purple rectangle**).

Table 4.3.1: Wavelength ranges of the defined band-pass filters.

No.	4-filter		5-filter		6-filter		7-filter	
	Ex [nm]	Em [nm]	Ex [nm]	Em [nm]	Ex [nm]	Em [nm]	Ex [nm]	Em [nm]
1	265~375	396~504	270~375	396~514	260~365	386~494	220~300	322~414
2	215~295	316~404	215~295	316~404	210~295	316~394	300~405	426~574
3	320~475	496~614	320~475	496~614	305~400	422~584	260~385	406~494
4	380~615	636~734	380~615	636~734	325~480	502~624	295~360	382~564
5			200~235	256~374	200~235	256~374	330~485	506~634
6					380~615	636~734	200~245	266~374
7							380~615	636~734

The results show that defined 4, 5, 6, and 7-filter sets cover the same or similar wavelength range. Each filter seems to represent common fluorescence peaks of several compounds. Filters 1, 2, 3, and 4 in the 4-filter set are the same or similar to filters 1, 2, 3, and 4 in the 5-filter set; and filters 3, 1, 5, and 7 in the 7-filter set. The first filter covers the fluorescence peaks for lycopene, NADH, NADPH, some vitamins (folic acid, menadione, and phytonadione), isoflavones (daidzein and formononetin), chlorogenic acid, eicosapentaenoic acid, ferulic acid, sinapinic acid, vanillin, and α-carotene. The second filter mainly covers the fluorescence peaks for ATP-related compounds (AMP, ADP, ATP, IMP, β-NAD+, and β-NADP+), amino acid (tryptophan, tyrosine, and phenylalanine), phenols (tyrosol and pyrocatechol), some vitamins (α-tocopherol, nicotinic acid, and pyridoxine), lignan (matairesinol and piroresinol), indole, and protocatechuic acid. The third filter mainly covers the fluorescence peaks for some vitamins (retinol, retinol acetate, riboflavin, and phytonadione). The last filter mainly covers the fluorescence peaks for some carotenoids (β-cryptoxanthin, chlorophyll a, and chlorophyll b), and doconexent.

Filter 5 in the 5-filter set are the same or similar to filters 5 in the 6-filter set; and filters 6 in the 7-filter set. This filter is close to filter 2 in the 4-filter set and therefore covers the fluorescence peaks for amino acid (part of tryptophan, tyrosine, and phenylalanine), phenols (tyrosol and pyrocatechol), some vitamins (α-tocopherol and part of pyridoxine), lignan (matairesinol and piroresinol), and indole. Filter 3 in the 6-filter set are the same or similar to filters 2 in the 7-filter set. Those filters overlap parts of filters 1 and 3 in the 4-filter set and therefore cover the fluorescence peaks for the same compounds. In addition, filters 3 in the 6-filter set covers the fluorescence peaks for caffeic acid (ethanol and phosphate solvent). The remaining filters in the 7-filter set is filter 4, which overlaps parts of filters 1 and 3 in the 4-filter set and therefore cover the fluorescence peaks for the same compounds. Besides, filters 4 in the 7-filter set covers the fluorescence peaks for caffeine.

4.3.2 Verifying the practicality of the proposed band-pass filters

The results of applying the band-pass filters to datasets for previous studies [21, 22, 62] are shown in Table 4.3.2. In this study, the EEM for the reagents was measured at 5 nm intervals for excitation wavelengths and 2 nm intervals for emission wavelengths. The results showed that all the defined band-pass filter sets have 5 nm intervals for excitation wavelengths and 2 nm intervals for emission wavelengths. However, the EEM datasets from previous studies were measured with 10 nm intervals [21, 22, 62]. Therefore, in this analysis, the wavelength range for band-pass filter were rounded to the nearest and larger wavelength range to cover the whole defined band-pass area. For example, filter 1 in the 4-filter for Ex = 265~375 nm, Em = 396~504 nm was rounded to Ex = 260~380 nm, Em = 390~510 nm in the 10 nm interval dataset. "All EEM" means that the entire EEM data after removing the scattering signals and non-fluorescence areas of the datasets [21, 22, 62] were used for analysis.

Table 4.3.2: Results of applying the defined band-pass filters to Nutmeg, Frozen fish and Mango dataset.

Dataset	**Nutmeg**	**Frozen fish**		**Mango**
Target	Aflatoxin contamination	K-value	IMP	Geographic origin
	R^2	R^2	R^2	Classification accuracy -%
Previous study	0.69 (all EEM*, 853)	0.78 (26)	0.82 (26)	92.30 (14)
All EEM*		0.91 (1 054)	0.87 (1 054)	91.92 (2 063)
4-filter (4)	0.69	0.30	0.78	70.69
5-filter (5)	0.68	0.31	0.78	83.11
6-filter (6)	0.68	0.69	0.80	83.12
7-filter (7)	0.71	0.56	0.84	82.20

* Analysis results using whole EEM data after removal of the scattering signals and non-fluorescence area.
** Numbers in ( ) along with R^2 or classification accuracy indicate number of variables used.

For the nutmeg dataset, the coefficient of determination (R^2) for predicting antitoxin contamination was 0.69 when using the 4-filter set, 0.68 when using the 5-filter set and 6-filter set, and 0.71 when using the 7-filter set, which are similar to the result obtained in the previous study (0.69) [21]. However, in the previous study, a whole EEM with 853 variables was used for prediction, and the number of variables was significantly higher than for the band-pass filters with four to seven variables used in the present study. According to the previous study [21], the variable importance in projection (VIP) value for the aflatoxin concentrations prediction model showed some peaks at Ex = 250, 320, 390, 460, and 520 nm, and Em = 420,

420, 490, 720, and 640 nm, where Ex = 250 nm / Em = 420 nm reflects the fluorescence of aflatoxin and Ex = 390 nm / Em = 490 nm reflects the fluorescence of kojic acid derivatives. These five excitation-emission areas are all covered or are very close to the wavelength range of the 4-filter, 5-filter, 6-filter and 7-filter sets. This explains why all types of filter showed similar performance as in the previous study [21].

For the frozen fish dataset, in predicting inosine 5'-monophosphate (IMP), the coefficient of determination of prediction was 0.78 when using the 4-filter set and 5-filter set, and 0.84 when using the 7-filter set, which is similar to the result of the previous study (0.82) [62]. In predicting the *K*-value, which is the freshness index of fish, the coefficient of determination for the prediction was 0.30 when using the 4-filter set, 0.30 when using the 5-filter set, 0.69 when using the 6-filter set, and 0.56 when using the 7-filter set, which are considerably worse than the results of the previous study (0.78) [62]. The *K*-value is calculated using the concentrations of six compounds, that is, adenosine 5'-triphosphate (ATP), 5'-diphosphate (ADP), adenosine 5'-monophosphate (AMP), IMP, inosine (HxR), and hypoxanthine (Hx) [43], where only ATP, ADP, AMP, and IMP emit fluorescence. In the previous study [62], the *K*-value was estimated by using the fluorescence image obtained at Ex = 340 nm, Em = 380~630 nm with a 10 nm interval. In the study by ElMasry et al. [14], the *K*-value was estimated using 11 excitation-emission combinations (Ex = 480 nm; Em = 550, 590, 610, 670, 700, 710, 730, 750, and 770 nm). In the present study, the fluorescence peak areas for ATP, ADP, AMP, and IMP were only covered by filters 1 and 2 in the 4-filter, 5-filter, and 6-filter sets; and filters 1 and 3 in the 7-filter set, which might have restricted the resolution. Hence, the predicted *K*-values were less accurate than those obtained in the previous study [62].

For the mango dataset, three localities in different geographical regions (Taiwan, Miyazaki, and Okinawa) were used as classification targets. The classification accuracy was 70.69 % when using the 4-filter set, 83.11 % when using the 5-filter set, 83.12 % when using the 6-filter set, and 82.20 % when using the 7-filter set. These accuracy values were less than those using the whole EEM (91.92 %) and the previous study (92.30 %) [22], but this is a reasonable accuracy for such a small number of filters. There were 14 combinations of excitation-emission wavelengths used for classification in the previous study, and the number of variables is significantly larger than the defined band-pass filters. In the previous study [22], it was suggested that the fluorescence information in the wavelength range of Ex = 260~290 nm and Em = 340~360 nm contributed significantly to the determination of the geographic origin for mangoes. This wavelength range was covered by filter 2 in the 4-filter, 5-filter, and 6-filter sets; and filter 1 in the 7-filter set, which suggests that these filter sets worked with reasonable accuracy for a smaller number of variables.

In this study, however, the performance of the proposed band-pass filters was not tested using actual

instruments, but only through simulations. This means that the camera sensitivity, filter transmittance, and environmental noise were not considered. These results show that the proposed band-pass filters have similar or practical accuracy to previously reported methods [21,22,62]. The prediction and classification accuracies are higher for the 5 to 7-filter set than for 4-filter set. Moreover, the filters were able to reduce the number of variables in the prediction model to seven variables or less, respectively, thereby reducing the measurement time and filter cost compared to applying the same wavelength combinations as in previous studies [21, 22, 62] to the fluorescence imaging system. This suggests that the proposed filters could be used as versatile filters for fluorescence imaging of food products for quality assessment. The experimental validation of the performance is a subject for future work.

Chapter 5

Conclusion

This thesis proposed a novel method to apply fluorescence as food quality assessment. This chapter summarized the main finding from two studies.

5.1 Contributions

The first study developed a novel approach for evaluating frozen fish quality and freshness by combining the fluorescence EEM with an imaging technique. Visualization was successfully performed to reveal the spatial-temporal changes of frozen fish quality such as K-value and IMP content with accuracy of $R^2 = 0.78$ and $R^2 = 0.82$, respectively using only one excitation light. The results also showed that the changing trends of both K-value and IMP content in fish differ between each part. Besides, this new method was applied to differentiate burnt meat and suggested that burnt meat could be detected even in a frozen condition. The proposed method offers a more practical way for large-scale commercial purposes. Further development will be needed to visualize the distribution of fish quality from the skin side, which will be a more pragmatic approach in actual use.

The second study proposed versatile band-pass filters for fluorescence imaging of the food product for quality assessment. The practical accuracy was achieved in most of the cases even though the number of auto-fluorescent compounds used in filter design was limited. Of course, if other auto-fluorescent compounds, such as plant pigments, are added to the filter design, a highly accurate filter can be created. However, the number of fluorescent compounds is enormous, and it is not realistic to measure all the fluorescent compounds. Thus, the top 100 compounds contained in food as listed by FooDB were tested. Therefore, the proposed band-pass filters cover the majority range of compounds contained in food. In addition, the

proposed band-pass filters were able to reduce the number of variables in the prediction model. In traditional methods, different wavelengths are chosen for different estimation targets in the calibration stage, thus, different band-pass filters are needed for different estimation targets, making fluorescence imaging a costly technique. If the same filters are employed for different targets, mass production and cost reductions, as have been achieved for filters for RGB cameras, can be expected. Therefore, this approach offers a more practical way of adopting fluorescence measurements for determining quality and authenticating food products than using target-specific filters.

5.2 Limitations and future perspectives

5.2.1 Measure fluorescence image without using a darkroom

The proposed imaging system uses fluorescence images, which are required to measure inside a darkroom. This is because the intensity of fluorescence is usually weak. Of course, there is a way to increase the fluorescence intensity of the target, for example, increasing the intensity of the excitation light by using a stronger light source. In this thesis, two Xenon light sources were used for measurement (Fig. 3.2.3). However, the intensity of fluorescence is still weaker than that of room light. As a future prospect, a technological development that can measure fluorescent images under the room light is required. The image-based reflective and fluorescent components separation method was proposed by Zhang et al. [70]. Although this is a separation of simple fluorescence properties and the and the result is an RGB image, not the spectral information, based on this study, the estimation of more complex fluorescence properties, such as those found in food, can be expected.

5.2.2 Larger dataset, better versatility

In this thesis, the versatile band-pass filters were defined base on a synthetic EEM dataset, which is generated from EEM of forty-one compounds. These compounds cover the majority range of fluorescent compounds contained in food, however, there are a vast number of fluorescent compounds in nature. Of course, if more auto-fluorescent compounds are added to the filter design, higher accuracy and higher versatile filters can be defined. On-going and future studies of EEM in foods will provide larger dataset, and allow us to apply on more extensive of food products and more complex estimation/classification tasks.

5.2.3 Imaging system with proposed versatile band-pass filters

This thesis verified the practicality of the proposed versatile band-pass filters with the three datasets related to food from the previous studies [21, 22, 62]. The ideal data that would be obtained by the proposed filters are simulated and then the accuracy of estimation/classification are calculated. This means that the camera sensitivity, filter transmittance, and actual experimental environment noise as described in Chapter 3, are not considered. For this reason, it is needed to build and validate an imaging system with proposed versatile band-pass filters.

5.2.4 Applications in other fields

This thesis presented the novel imaging method using fluorescence, and presented versatile band-pass filters made suitable for their introduction in the food industry. The proposed imaging method can be widely used not only for food, however the versatile band-pass filters are food-specific. By adding more fluorescent compounds to the dataset or using new dataset related to other fields to re-defined the versatile band-pass filters, the proposed method is expected to be able applied to fields other than food.

Bibliography

[1] J. Christensen, L. Nørgaard, R. Bro, and S. B. Engelsen, "Multivariate autofluorescence of intact food systems," *Chemical Reviews*, vol. 106, no. 6, pp. 1979–1994, 2006.

[2] M. Iwamoto, S. Kawano, and J. Uozumi, "An introduction to the near equatorial spectral method (in Japanese)," *Saiwaishobo*, pp. 45–46, 1994.

[3] I. M. Warner, G. D. Christian, E. R. Davidson, and J. B. Callis, "Analysis of multicomponent fluorescence data," *Analytical Chemistry*, vol. 49, no. 4, pp. 564–573, 1977.

[4] M. J. Sorrell, J. Tribble, L. Reinisch, J. A. Werkhaven, and R. H. Ossoff, "Bacteria identification of otitis media with fluorescence spectroscopy," *Lasers in Surgery and Medicine*, vol. 14, no. 2, pp. 155–163, 1994.

[5] G. Wolf, J. S. Almeida, C. Pinheiro, V. Correia, C. Rodrigues, M. A. M. Reis, and J. G. Crespo, "Two-dimensional fluorometry coupled with artificial neural networks: A novel method for on-line monitoring of complex biological processes," *Biotechnology and Bioengineering*, vol. 72, no. 3, pp. 297–306, 2001.

[6] H. J. C. M. Sterenborg, M. Motamedi, R. F. Wagner, M. Duvic, S. Thomsen, and S. L. Jacques, "In vivo fluorescence spectroscopy and imaging of human skin tumours," *Lasers in Medical Science*, vol. 9, no. 3, pp. 191–201, 1994.

[7] J. A. Werkhaven, L. Reinisch, M. Sorrell, J. Tribble, and R. H. Ossoff, "Noninvasive optical diagnosis of bacteria causing otitis media," *The Laryngoscope*, vol. 104, no. 3, pp. 264–268, 1994.

[8] R. Karoui and C. Blecker, "Fluorescence spectroscopy measurement for quality assessment of food systems - A review," *Food and Bioprocess Technology*, vol. 4, no. 3, pp. 364–386, 2011.

[9] J. Tsujiuchi, K. Kuroda, H. Oki, S. Kawata, T. Kojima, M. Takeda, S. Minami, T. Yatagai, and M. Yamamoto, *The latest optical technology handbook (in Japanese)*. Asakura Publising Co., Ltd., 2012.

[10] J. K. S. Møller, G. Parolari, L. Gabba, J. Christensen, and L. H. Skibsted, "Monitoring chemical changes of dry-cured parma ham during processing by surface autofluorescence spectroscopy," *Journal of Agricultural and Food Chemistry*, vol. 51, no. 5, pp. 1224–1230, 2003.

[11] P. O. Skjervold, R. G. Taylor, J. P. Wold, P. Berge, S. Abouelkaram, J. Culioli, and E. Dufour, "Development of intrinsic fluorescent multispectral imagery specific for fat, connective tissue, and myofibers in meat," *Journal of Food Science*, vol. 68, no. 4, pp. 1161–1168, 2003.

[12] E. Olsen, G. Vogt, D. Ekeberg, M. Sandbakk, J. Pettersen, and A. Nilsson, "Analysis of the early stages of lipid oxidation in freeze-stored pork back fat and mechanically recovered poultry meat," *Journal of Agricultural and Food Chemistry*, vol. 53, no. 2, pp. 338–348, 2005.

[13] É. Dufour, J. P. Frencia, and E. Kane, "Development of a rapid method based on front-face fluorescence spectroscopy for the monitoring of fish freshness," *Food Research International*, vol. 36, no. 5, pp. 415–423, 2003.

[14] G. ElMasry, H. Nagai, K. Moria, N. Nakazawa, M. Tsuta, J. Sugiyama, E. Okazaki, and S. Nakauchi, "Freshness estimation of intact frozen fish using fluorescence spectroscopy and chemometrics of excitation-emission matrix," *Talanta*, vol. 143, pp. 145–156, 2015.

[15] G. ElMasry, N. Nakazawa, E. Okazaki, and S. Nakauchi, "Non-invasive sensing of freshness indices of frozen fish and fillets using pretreated excitation-emission matrices," *Sensors and Actuators B: Chemical*, vol. 228, pp. 237–250, 2016.

[16] M. Shibata, G. ElMasry, K. Moriya, M. M. Rahman, Y. Miyamoto, K. Ito, N. Nakazawa, S. Nakauchi, and E. Okazaki, "Smart technique for accurate monitoring of ATP content in frozen fish fillets using fluorescence fingerprint," *LWT - Food Science and Technology*, vol. 92, pp. 258–264, 2018.

[17] R. Karoui, B. Kemps, F. Bamelis, B. De Ketelaere, K. Merten, R. Schoonheydt, E. Decuypere, and J. De Baerdemaeker, "Development of a rapid method based on front face fluorescence spectroscopy for the monitoring of egg freshness: 1 - evolution of thick and thin egg albumens," *European Food Research and Technology*, vol. 223, no. 3, pp. 303–312, 2006.

[18] R. Karoui, B. Kemps, F. Bamelis, B. De Ketelaere, K. Merten, R. Schoonheydt, E. Decuypere, and J. De Baerdemaeker, "Development of a rapid method based on front-face fluorescence spectroscopy for the monitoring of egg freshness: 2 - evolution of egg yolk," *European Food Research and Technology*,

vol. 223, no. 2, pp. 180–188, 2006.

[19] M. C. Codrea, O. S. Nevalainen, E. Tyystjärvi, M. Vandeven, and R. Valcke, "Classifying apples by the means of fluorescence imaging," *International Journal of Pattern Recognition and Artificial Intelligence*, vol. 18, no. 02, pp. 157–174, 2004.

[20] I. U. Bron, R. V. Ribeiro, M. Azzolini, A. P. Jacomino, and E. C. Machado, "Chlorophyll fluorescence as a tool to evaluate the ripening of 'golden' papaya fruit," *Postharvest Biology and Technology*, vol. 33, no. 2, pp. 163–173, 2004.

[21] R. Aiyama, V. Trivittayasil, and M. Tsuta, "Discrimination of aflatoxin contamination level in nutmeg by fluorescence fingerprint measurement," *Food control*, vol. 85, pp. 113–118, 2018.

[22] Y. Nakamura, K. Fujita, J. Sugiyama, M. Tsuta, M. Shibata, M. Yoshimura, M. Kokawa, H. Nabetani, and T. Araki, "Discrimination of the geographic origin of mangoes using fluorescence fingerprint," *Journal of the Japanese Society for Food Science and Technology*, vol. 59, no. 8, pp. 387–393, 2012.

[23] V. Trivittayasil, M. Tsuta, S. Kasai, Y. Matsuo, Y. Sekiyama, T. Shoji, R. Aiyama, M. Kokawa, and J. Sugiyama, "Classification of 1-methylcyclopropene treated apples by fluorescence fingerprint using partial least squares discriminant analysis with stepwise selectivity ratio variable selection method," *Chemometrics and Intelligent Laboratory Systems*, vol. 175, pp. 30–36, 2018.

[24] M. Zandomeneghi, L. Carbonaro, and C. Caffarata, "Fluorescence of vegetable oils: olive oils," *Journal of agricultural and food chemistry*, vol. 53, no. 3, pp. 759–766, 2005.

[25] E. Sikorska, A. Romaniuk, I. V. Khmelinskii, R. Herance, J. L. Bourdelande, M. Sikorski, and J. Kozioł, "Characterization of edible oils using total luminescence spectroscopy," *Journal of Fluorescence*, vol. 14, no. 1, pp. 25–35, 2004.

[26] F. Guimet, J. Ferré, R. Boqué, and F. X. Rius, "Application of unfold principal component analysis and parallel factor analysis to the exploratory analysis of olive oils by means of excitation–emission matrix fluorescence spectroscopy," *Analytica Chimica Acta*, vol. 515, no. 1, pp. 75–85, 2004.

[27] F. Guimet, R. Boqué, and J. Ferré, "Cluster analysis applied to the exploratory analysis of commercial Spanish olive oils by means of excitation- emission fluorescence spectroscopy," *Journal of agricultural and food chemistry*, vol. 52, no. 22, pp. 6673–6679, 2004.

[28] K. Apperson, K. A. Leiper, I. P. McKeown, and D. J. Birch, "Beer fluorescence and the isolation, characterisation and silica adsorption of haze-active beer proteins," *Journal of the Institute of Brewing*, vol. 108, no. 2, pp. 193–199, 2002.

[29] E. Sikorska, T. Górecki, I. V. Khmelinskii, M. Sikorski, and D. De Keukeleire, "Fluorescence spectroscopy for characterization and differentiation of beers," *Journal of the Institute of Brewing*, vol. 110, no. 4, pp. 267–275, 2004.

[30] J. Christensen, A. M. Ladefoged, and L. Nørgaard, "Rapid determination of bitterness in beer using fluorescence spectroscopy and chemometrics," *Journal of the Institute of Brewing*, vol. 111, no. 1, pp. 3–10, 2005.

[31] E. Sikorska, T. Górecki, I. V. Khmelinskii, M. Sikorski, and D. De Keukeleire, "Monitoring beer during storage by fluorescence spectroscopy," *Food Chemistry*, vol. 96, no. 4, pp. 632–639, 2006.

[32] M. Insinska-Rak, E. Sikorska, I. Czerwinska, A. Kruzinska, G. Nowacka, and M. Sikorski, "Fluorescence spectroscopy for analysis of beer," *Polish Journal of Food and Nutrition Sciences*, vol. 57, no. 4 [B], 2007.

[33] L. M. Nollet and F. Toldrá, *Handbook of seafood and seafood products analysis*. CRC Press, 2009.

[34] G. Olafsdottir, E. Martinsdóttir, J. Oehlenschläger, P. Dalgaard, B. Jensen, I. Undeland, I. M. Mackie, G. Henehan, J. Nielsen, and H. A. Nilsen, "Methods to evaluate fish freshness in research and industry," *Trends in Food Science & Technology*, vol. 8, no. 8, pp. 258–265, 1997.

[35] X. Huang, J. Xin, and J. Zhao, "A novel technique for rapid evaluation of fish freshness using colorimetric sensor array," *Journal of Food Engineering*, vol. 105, no. 4, pp. 632–637, 2011.

[36] L. F. Jacober and A. G. Rand, "Biochemical evaluation of seafood," *Chemistry and Biochemistry of Marine Food Products*, pp. 347–365, 1982.

[37] M. E. Surette, T. A. Gill, and P. J. LeBlanc, "Biochemical basis of postmortem nucleotide catabolism in cod (Gadus morhua) and its relationship to spoilage," *Journal of Agricultural and Food Chemistry*, vol. 36, no. 1, pp. 19–22, 1988.

[38] T. A. Gill, "Objective analysis of seafood quality," *Food Reviews International*, vol. 6, no. 4, pp. 681–714, 1990.

[39] D. H. Greene, J. K. Babbitt, and K. D. Reppond, "Patterns of nucleotide catabolism as freshness indicators in flatfish from the Gulf of Alaska," *Journal of Food Science*, vol. 55, no. 5, pp. 1236–1238, 1990.

[40] T. Haitula, M. Kiesvaara, and M. Moran, "Freshness evaluation in European whitefish (Coregonus wartmanni) during chill storage," *Journal of Food Science*, vol. 58, no. 6, pp. 1212–1215, 1993.

[41] C. Handumrongkul and J. Silva, "Aerobic counts, color and adenine nucleotide changes in CO2 packed refrigerated striped bass strips," *Journal of Food Science*, vol. 59, no. 1, pp. 67–69, 1994.

[42] H. Hong, J. M. Regenstein, and Y. Luo, "The importance of ATP-related compounds for the freshness and flavor of post-mortem fish and shellfish muscle: A review," *Critical Reviews in Food Science and Nutrition*, vol. 57, no. 9, pp. 1787–1798, 2017.

[43] T. Saito, "A new method for estimating the freshness of fish," *Bulletin of the Japanese Society for the Science of Fish*, vol. 24, pp. 749–750, 1959.

[44] M. Ando, M. Joka, S. Mochizuki, K.-I. Satoh, Y. Tsukamasa, and Y. Makinodan, "Influence of death struggle on the structural changes in chub mackerel muscle during chilled storage," *Fisheries Science*, vol. 67, no. 4, pp. 744–751, 2001.

[45] C. Watson, R. E. Bourke, and R. W. Brill, "A comprehensive theory on the etiology of burnt tuna," *Fishery Bulletin*, vol. 86, no. 2, pp. 367–372, 1988.

[46] S. Ehira, K. Saito, and H. Uchiyama, "Accurracy of measuring K value, an index for estimating freshness of fish, by freshness testing paper," *Bulletin of Tokai Regional Fisheries Research Laboratory (Japan)*, 1986.

[47] T. Maeda, A. Yuki, H. Sakurai, K. Watanabe, N. Itoh, E. Inui, K. Seike, Y. Mizukami, Y. Fukuda, and K. Harada, "Alcohol brine freezing of japanese horse mackerel (Trachurus japonicus) for raw consumption," *Transactions of the Japan Society of Refrigerating and Air Conditioning Engineers*, vol. 24, no. 4, pp. 323–330, 2007.

[48] H. Nasibov, A. Kholmatov, B. Akselli, A. Nasibov, and S. Baytaroglu, "Performance analysis of the CCD pixel binning option in particle-image velocimetry measurements," *IEEE/ASME Transactions on Mechatronics*, vol. 15, no. 4, pp. 527–540, 2010.

[49] J. Sugiyama, "Visualization of sugar content in the flesh of a melon by near-infrared imaging," *Journal of Agricultural and Food Chemistry*, vol. 47, no. 7, pp. 2715–2718, 1999.

[50] M. Tsuta, J. Sugiyama, and Y. Sagara, "Near-infrared imaging spectroscopy based on sugar absorption band for melons," *Journal of Agricultural and Food Chemistry*, vol. 50, no. 1, pp. 48–52, 2002.

[51] B. Valeur and J.-C. Brochon, *New trends in fluorescence spectroscopy: applications to chemical and life sciences*, vol. 1. Springer Science & Business Media, 2012.

[52] Å. Rinnan and C. M. Andersen, "Handling of first-order Rayleigh scatter in PARAFAC modelling of fluorescence excitation–emission data," *Chemometrics and Intelligent Laboratory Systems*, vol. 76, no. 1, pp. 91–99, 2005.

[53] C. M. Andersen and R. Bro, "Practical aspects of PARAFAC modeling of fluorescence excitation-emission data," *Journal of Chemometrics*, vol. 17, no. 4, pp. 200–215, 2003.

[54] K. Fijisawa and M. Yoshino, "Activities of adenylate-degrading enzymes in muscles from vertebrates and invertebrates," *Comparative Biochemistry and Physiology Part B: Biochemistry and Molecular Biology*, vol. 86, no. 1, pp. 109–112, 1987.

[55] N. Jones and J. Murray, "Rapid measures of nucleotide dephosphorylation in iced fish muscle. their value as indices of freshness and of inosine 5'-monophosphate concentration," *Journal of the Science of Food and Agriculture*, vol. 15, no. 10, pp. 684–690, 1964.

[56] K. Yukitoshi, K. Ai, H. Mie, and I. Yukio, "Studies on the "Yakeniku" of Thunnus thynnus unloaded at the Sakaiminato fishing port (in Japanese)," *Tottori Institute of Industrial Technology Research Report*, vol. 2010, no. 13, pp. 1–10, 2010.

[57] E. Olsen, A. Veberg, G. Vogt, O. Tomic, B. Kirkhus, D. Ekeberg, and A. Nilsson, "Analysis of early lipid oxidation in salmon pâté with cod liver oil and antioxidants," *Journal of Food Science*, vol. 71, no. 3, pp. S284–S292, 2006.

[58] K. Hasegawa, Y. Endo, and K. Fujimoto, "Oxidative deterioration in dried fish model systems assessed by solid sample fluorescence spectrophotometry," *Journal of Food Science*, vol. 57, no. 5, pp. 1123–1126, 1992.

[59] I. Birlouez-Aragon, M. Nicolas, A. Metais, N. Marchond, J. Grenier, and D. Calvo, "A rapid fluorimet-

ric method to estimate the heat treatment of liquid milk," *International Dairy Journal*, vol. 8, no. 9, pp. 771–777, 1998.

[60] S. P. Aubourg, C. G. Sotelo, and R. Pérez-Martín, "Assessment of quality changes in frozen sardine (sardina pilchardus) by fluorescence detection," *Journal of the American Oil Chemists' Society*, vol. 75, no. 5, pp. 575–580, 1998.

[61] K. Nishino, K. Nakamura, M. Tsuta, M. Yoshimura, J. Sugiyama, and S. Nakauchi, "Optimization of excitation-emission band-pass filter for visualization of viable bacteria distribution on the surface of pork meat," *Optics Express*, vol. 21, no. 10, pp. 12579–12591, 2013.

[62] M. V. Bui, M. M. Rahman, N. Nakazawa, E. Okazaki, and S. Nakauchi, "Visualize the quality of frozen fish using fluorescence imaging aided with excitation-emission matrix," *Optics Express*, vol. 26, no. 18, pp. 22954–22964, 2018.

[63] M. Ram, L. M. Seitz, and F. E. Dowell, "Natural fluorescence of red and white wheat kernels," *Cereal Chemistry*, vol. 81, no. 2, pp. 244–248, 2004.

[64] R. A. Harshman, "Foundations of the PARAFAC procedure: Models and conditions for an "explanatory" multimodal factor analysis," *UCLA Working Papers in Phonetics*, vol. 16, no. 10,085, pp. 1–84, 1970.

[65] J. D. Carroll and J.-J. Chang, "Analysis of individual differences in multidimensional scaling via an N-way generalization of "eckart-young" decomposition," *Psychometrika*, vol. 35, no. 3, pp. 283–319, 1970.

[66] R. Bro and H. A. Kiers, "A new efficient method for determining the number of components in PARAFAC models," *Journal of Chemometrics: A Journal of the Chemometrics Society*, vol. 17, no. 5, pp. 274–286, 2003.

[67] K. R. Murphy, C. A. Stedmon, D. Graeber, and R. Bro, "Fluorescence spectroscopy and multi-way techniques. PARAFAC," *Analytical Methods*, vol. 5, no. 23, pp. 6557–6566, 2013.

[68] R. A. Harshman and M. E. Lundy, "PARAFAC: Parallel factor analysis," *Computational Statistics & Data Analysis*, vol. 18, no. 1, pp. 39–72, 1994.

[69] A. Savitzky and M. J. E. Golay, "Smoothing and differentiation of data by simplified least squares

procedures," *Analytical Chemistry*, vol. 36, no. 8, pp. 1627–1639, 1964.

[70] C. Zhang and I. Sato, "Image-based separation of reflective and fluorescent components using illumination variant and invariant color," *IEEE transactions on pattern analysis and machine intelligence*, vol. 35, no. 12, pp. 2866–2877, 2012.

Appendix A

Table A.1: List of compounds used in the experiment (1/3).

No.	CAS No.	Name	Company	Fluorescence	Solvent	Concentration (ppm)	Photomultiplier (V)
1	10191-41-0	(±)-α-Tocopherol	FUJIFILM Wako Pure Chemical Corporation	yes	ethanol	10	600
2	16178-48-6	ADP disodium salt	Oriental Yeast Co., Ltd.	yes	phosphate	100	100
3	18422-05-4	AMP	Oriental Yeast Co., Ltd.	yes	Mili-Q	100	900
4	520-36-5	Apigenin	FUJIFILM Wako Pure Chemical Corporation	none			
5	51963-61-2	ATP disodium salt hydrate	Oriental Yeast Co., Ltd.	yes	Mili-Q	100	800
6	58-85-5	Biotin	Sigma-Aldrich	none			
7	331-39-5	Caffeic acid	FUJIFILM Wako Pure Chemical Corporation	yes	ethanol	100	800
				yes	phosphate	100	900
8	58-08-2	Caffeine	FUJIFILM Wako Pure Chemical Corporation	yes	phosphate	100	900
9	327-97-9	Chlorogenic acid	FUJIFILM Wako Pure Chemical Corporation	yes	ethanol	100	800
10	479-61-8	Chlorophyll a	FUJIFILM Wako Pure Chemical Corporation	yes	ethanol	10	500
11	519-62-0	Chlorophyll b	Sigma-Aldrich	yes	ethanol	10	600
12	67-97-0	Cholecalciferol	FUJIFILM Wako Pure Chemical Corporation	none			
13	68-19-9	Cyanocobalamin	Sigma-Aldrich	none			
14	486-66-8	Daidzein	FUJIFILM Wako Pure Chemical Corporation	yes	phosphate	100	800
15	552-66-9	Daidzin	FUJIFILM Wako Pure Chemical Corporation	none			
16	6893-26-1	D-Glutamic acid	FUJIFILM Wako Pure Chemical Corporation	none			
17	6217-54-5	Doconexent	Sigma-Aldrich	yes	ethanol	100	800
18	10417-94-4	Eicosapentaenoic acid	Sigma-Aldrich	yes	ethanol	100	900
19	50-14-6	Ergocalciferol	FUJIFILM Wako Pure Chemical Corporation	none			
20	1135-24-6	Ferulic acid	FUJIFILM Wako Pure Chemical Corporation	yes	phosphate	100	800
21	59-30-3	Folic aid	FUJIFILM Wako Pure Chemical Corporation	yes	phosphate	100	900
22	485-72-3	Formononetin	Sigma-Aldrich	yes	ethanol	10	700
23	446-72-0	Genistein	FUJIFILM Wako Pure Chemical Corporation	none			
24	529-59-9	Genistin	Sigma-Aldrich	none			
25	617-65-2	Glutamic acid	FUJIFILM Wako Pure Chemical Corporation	none			

Table A.2: List of compounds used in the experiment (2/3).

No.	CAS No.	Name	Company	Fruorescence	Solvent	Concentration (ppm)	Photomultilier (V)
26	85-32-5	Guanylic acid	Combi-Blocks	none			
27	68-94-0	Hypoxanthine	FUJIFILM Wako Pure Chemical Corporation	none			
28	131-99-7	IMP	Junsei Chemical Co. Ltd.	yes	Mili-Q	100	900
29	120-72-9	Indole	FUJIFILM Wako Pure Chemical Corporation	yes	phosphate	100	500
30	58-63-9	Inosine	Junsei Chemical Co. Ltd.	none			
31	520-18-3	Kaempferol	FUJIFILM Wako Pure Chemical Corporation	none			
32	50-81-7	L(+)-Ascorbic acid	FUJIFILM Wako Pure Chemical Corporation	none			
33	61-90-5	Leucine	FUJIFILM Wako Pure Chemical Corporation	none			
34	56-86-0	L-Glutamic acid	FUJIFILM Wako Pure Chemical Corporation	none			
35	71-00-1	L-Histidine	FUJIFILM Wako Pure Chemical Corporation	none			
36	73-32-5	L-Isoleucine	FUJIFILM Wako Pure Chemical Corporation	none			
37	63-68-3	L-Methionine	FUJIFILM Wako Pure Chemical Corporation	none			
38	147-85-3	L-Proline	FUJIFILM Wako Pure Chemical Corporation	none			
39	73-22-3	L-Tryptophan	FUJIFILM Wako Pure Chemical Corporation	yes	phosphate	10	600
40	491-70-3	Luteolin	FUJIFILM Wako Pure Chemical Corporation	none			
41	502-65-8	Lycopene	FUJIFILM Wako Pure Chemical Corporation	yes	acetonitrile	1	900
42	56-87-1	Lysine	FUJIFILM Wako Pure Chemical Corporation	none			
43	580-72-3	Matairesinol	Sigma-Aldrich	yes	ethanol	10	600
44	58-27-5	Menadione	FUJIFILM Wako Pure Chemical Corporation	yes	ethanol	100	800
45	529-44-2	Myricetin	FUJIFILM Wako Pure Chemical Corporation	none			
46	606-68-8	NADH	Oriental Yeast Co., Ltd.	yes	phosphate	100	800
47	2646-71-1	NADPH	Combi-Blocks	yes	phosphate	100	800
48	98-92-0	Niacinamide	FUJIFILM Wako Pure Chemical Corporation	none			
49	59-67-6	Nicotinic acid	FUJIFILM Wako Pure Chemical Corporation	yes	ethanol	100	900
50	63-91-2	Phenylalanine	Peptide Institute, Inc.	yes	phosphate	100	800

Table A.3: List of compounds used in the experiment (3/3).

No.	CAS No.	Name	Company	Fruorescence	Solvent	Concentration (ppm)	Photomultilier (V)
51	84-80-0	Phytonadione	FUJIFILM Wako Pure Chemical Corporation	yes	ethanol	100	900
52	487-36-5	Pinoresinol	Sigma-Aldrich	yes	acetonitrile	10	500
53	99-50-3	Protocatechuic acid	FUJIFILM Wako Pure Chemical Corporation	yes	ethanol	10	600
54	65-23-6	Pyridoxine	Sigma-Aldrich	yes	ethanol	10	600
				yes	phosphate	10	600
55	120-80-9	Pyrocatechol	FUJIFILM Wako Pure Chemical Corporation	yes	phosphate	10	700
56	68-26-8	Retinol	Sigma-Aldrich	yes	ethanol	10	800
57	127-47-9	Retinol acetate	FUJIFILM Wako Pure Chemical Corporation	yes	ethanol	10	800
58	83-88-5	Riboflavine	Sigma-Aldrich	yes	phosphate	100	600
59	530-59-6	Sinapinic acid	Sigma-Aldrich	yes	phosphate	100	900
60	83-67-0	Theobromine	FUJIFILM Wako Pure Chemical Corporation	none			
61	24539	Thiamine hydrochloride	FUJIFILM Wako Pure Chemical Corporation	none			
62	72-19-5	Threonine	FUJIFILM Wako Pure Chemical Corporation	none			
63	60-18-4	Tyrosine	FUJIFILM Wako Pure Chemical Corporation	yes	phosphate	10	600
64	501-94-0	Tyrosol	FUJIFILM Wako Pure Chemical Corporation	yes	phosphate	10	600
65	72-18-4	Valine	FUJIFILM Wako Pure Chemical Corporation	none			
66	121-33-5	Vanillin	FUJIFILM Wako Pure Chemical Corporation	yes	ethanol	100	900
67	137-08-6	Vitamin B5	FUJIFILM Wako Pure Chemical Corporation	none			
68	144-68-3	Zeaxanthin	Sigma-Aldrich	none			
69	7488-99-5	α-Carotene	FUJIFILM Wako Pure Chemical Corporation	yes	ethanol	10	900
70	472-70-8	β-Cryptoxanthin	FUJIFILM Wako Pure Chemical Corporation	yes	acetonitrile	1	900
71	53-84-9	β-NAD+	Oriental Yeast Co., Ltd.	yes	Mili-Q	100	900
72	1184-16-3	β-NADP+	Oriental Yeast Co., Ltd.	yes	Mili-Q	100	900

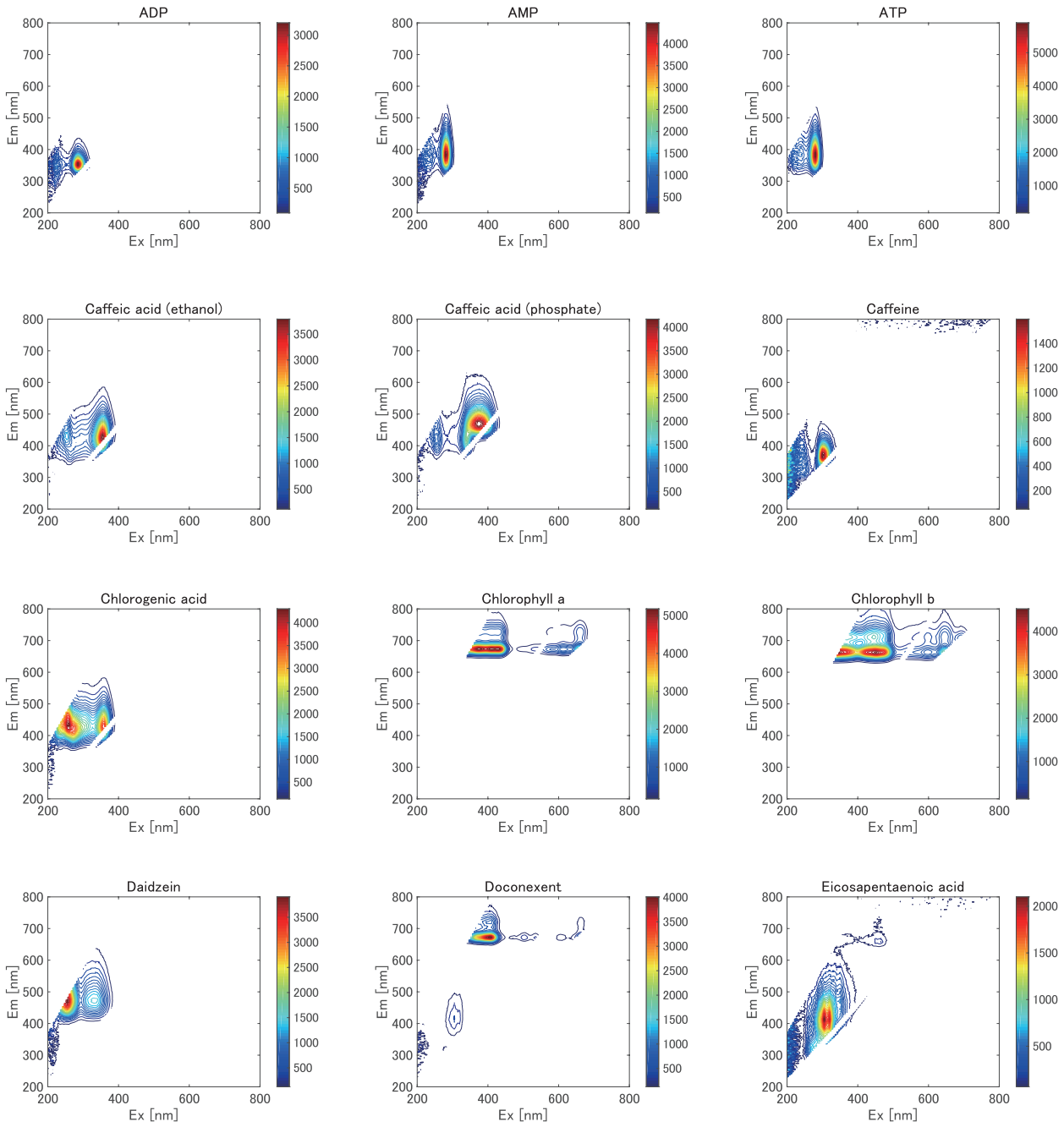

Fig. A.1: EEM of compounds emitted fluorescence (1/4).

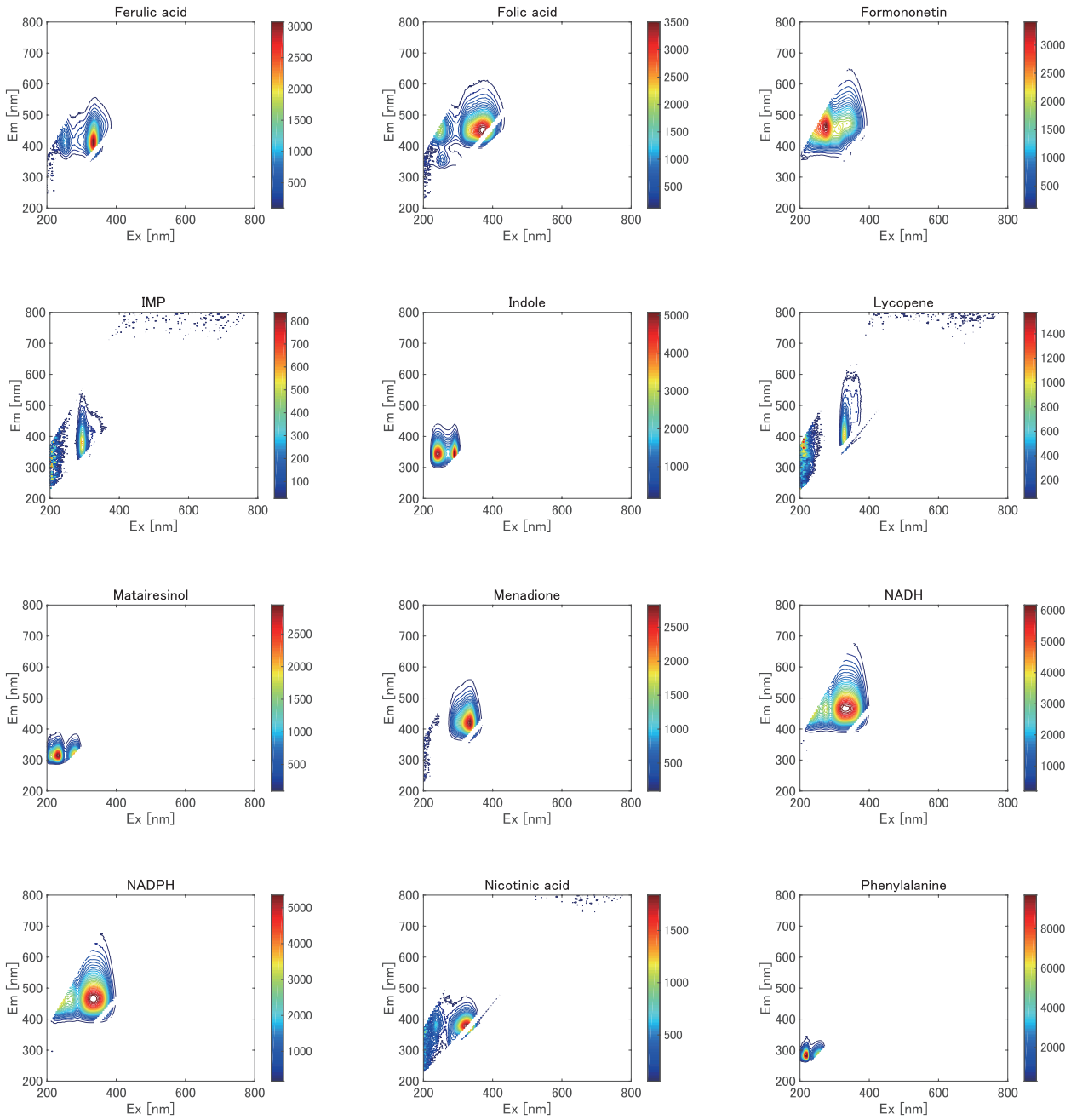

Fig. A.2: EEM of compounds emitted fluorescence (2/4).

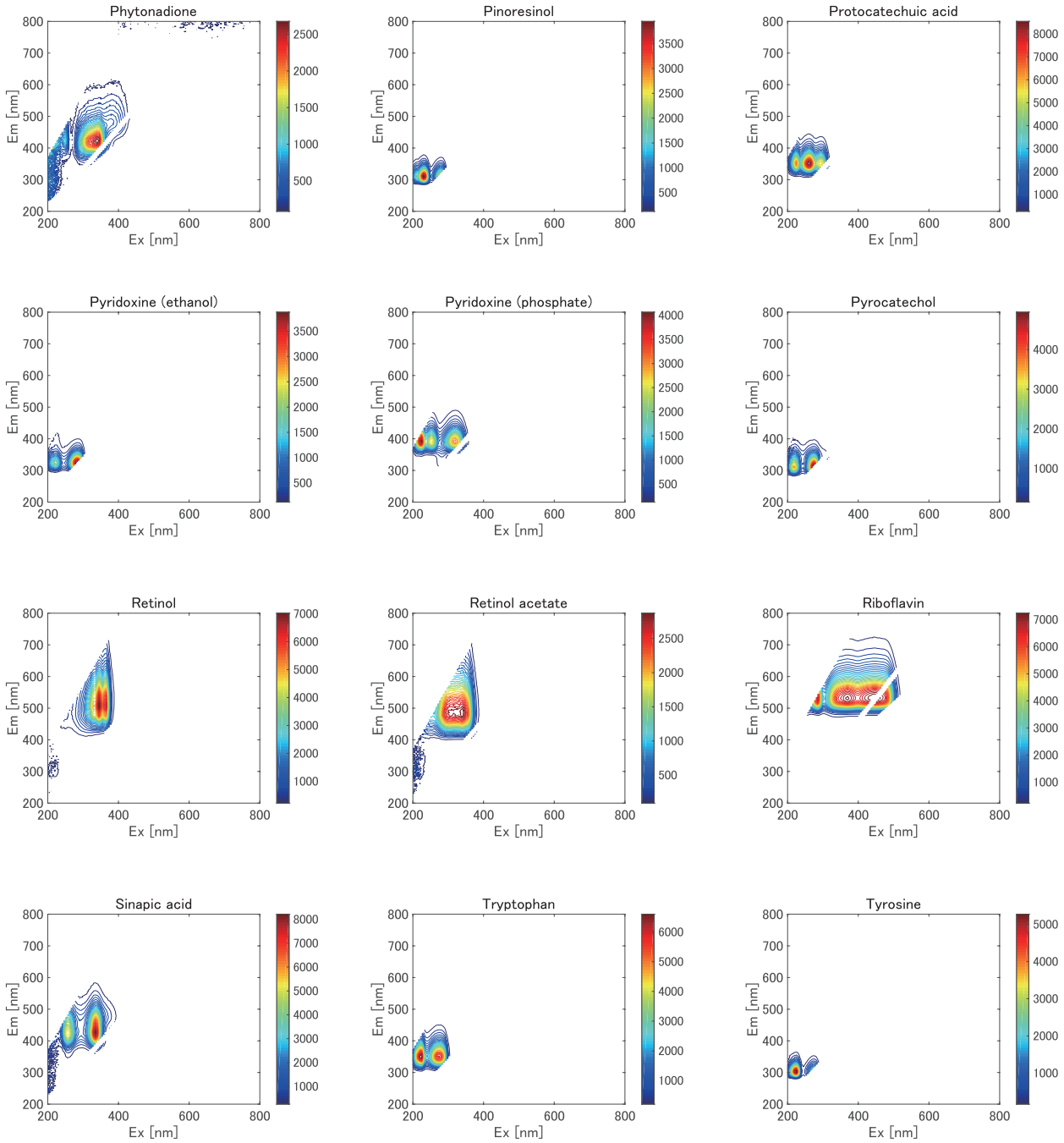

Fig. A.3: EEM of compounds emitted fluorescence (3/4).

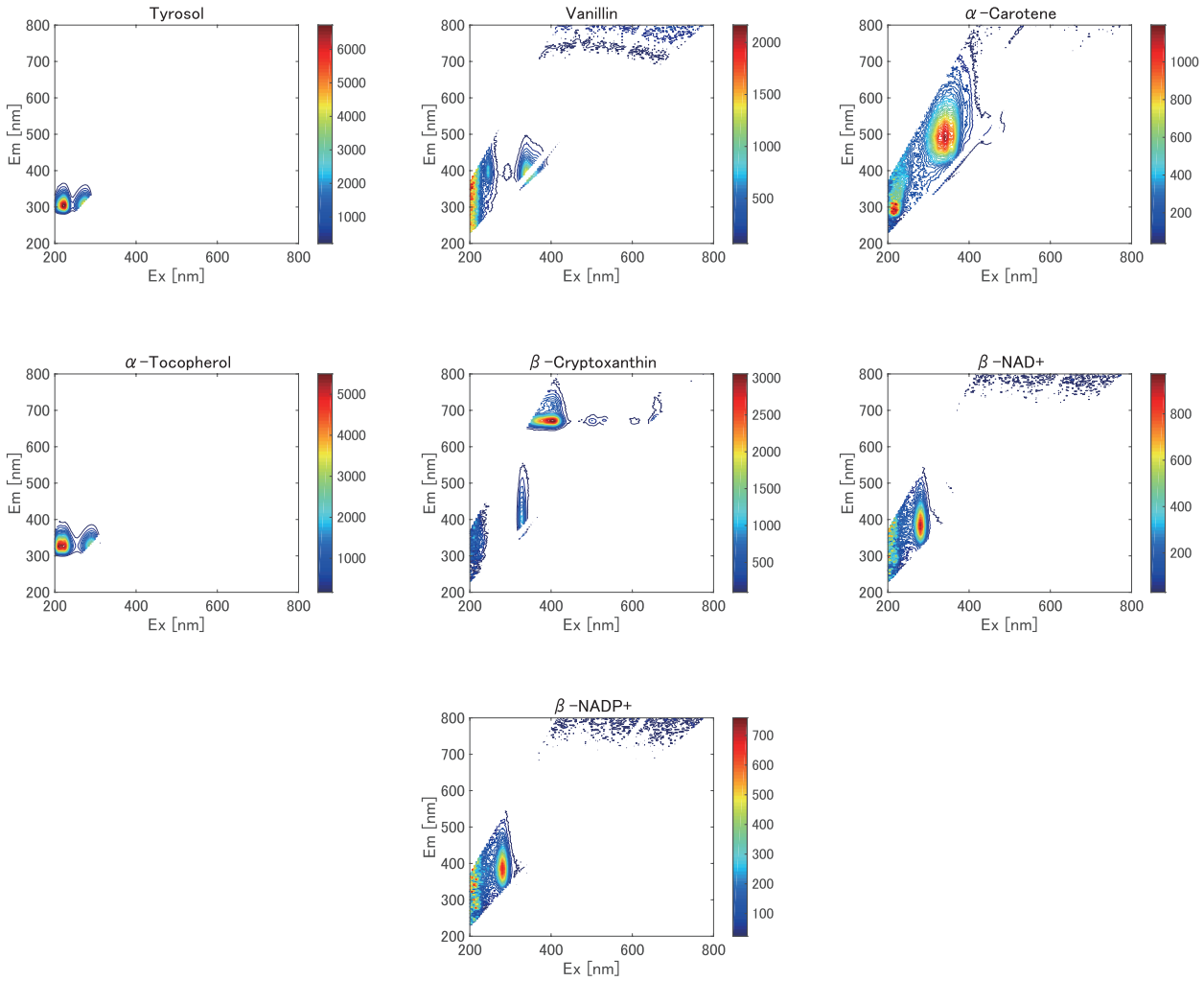

Fig. A.4: EEM of compounds emitted fluorescence (4/4).